Application Meshless Method for Fracture Crack Growth Analysis

By

Kamal Sharma

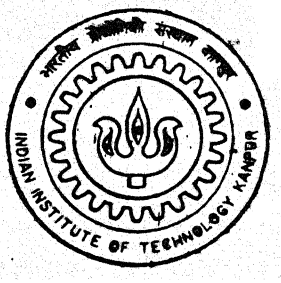

DEPARTMENT OF MECHANICAL ENGINEERING

Indian Institute of Technology Kanpur

August, 2002

Application of Meshless Method for Fracture Crack Growth Analysis

A Thesis Submitted
In Partial Fulfilment of the Requirement
For the Degree
of

Master of Technology

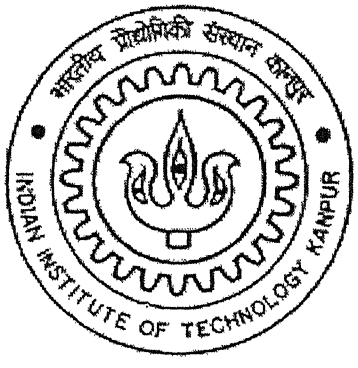

by

Kamal Sharma

(NET-Y011503)

Department of Mechanical Engineering

Indian Institute of Technology

Kanpur-208016, India

August-2002

CERTIFICATE

It is certified that the work contained in this thesis entitled ***"Application Of Meshless Method for Fracture Crack Growth Analysis"***, by ***Mr. Kamal Sharma*** has been carried out under my supervision and that work has not been submitted elsewhere for a degree.

N N Kishore

Dr. N.N.Kishore
Professor
Dept. of Mechanical Engineering
I. I. T. Kanpur

August, 2002

CONTENTS

Conclusions

LIST OF FIGURES

LIST OF TABLES

Dedicated
To
Well-Wishers

Abstract

Element free Galerkin (EFG) method is a computational tool in solid mechanics problem for solving partial differential equations based on a scattered set of nodal points. This method belongs to the class of meshless methods, which is particularly useful for problems involving crack propagation due to the absence of any predefined element connectivity, and the burdensome remeshing required as in finite element method (FEM). This method is based on the use of moving least square Interpolants with a Galerkin method. In the present problem, the implementation of EFG method for problem of fracture and quasi static crack growth is described. Numerical results show that accurate stress intensity factor can be obtained without any enrichment of displacement field near the crack tip. The stress singularity and the crack growth can be easily modeled. In this crack propagation problem in plane elasticity is considered. Lastly, the problem of propagation of multiple, arbitrarily placed, crack is considered.

Acknowledgements

As my academic career draws to a close, there are many people who have been a great help to me along the way and I would like to thank them here. First of all, I would like to thank my guide, ***Prof. N. N. Kishore*** for all his persistent guidance along the way. I would also like to thank ***Dr. V. B. Shenoy***, helping throughout my stay at IITK.

I was very fortunate to have many good friends and colleagues in IIT and if space permitted I would write a volume on each one. However, that is not the case, so I will simply mention the name and want to say a word of thanks to my ***A-TOP friends Gaurav, Suresh, Jeetu, Jeevan & Pawan***. Without their motivation and help I would have never come this far. Thanks to the guys from my era with whom I had many useful discussions of research, sports and many other subjects: ***Gajju, Tarun, Avi & guptaank.*** Good luck to the "young" guys who came after me and still have a little ways to go.

Thanks to my parents for always being they're for me. They are cheering me up when the pressures of thesis and courses was heavy on me.

Finally, I would like to thanks to my dear wife ***Babita*** for helping me out so much as I finished M.Tech. and wrote my thesis. She took care of everything so I could concentrate on my thesis. I have never experienced such unweaving love and supports. She was my best '***discovery***' in IIT career and I dedicated this thesis to her also.

CHAPTER 1

INTRODUCTION

1.1 INTRODUCTION

For the many structures, crack propagation is an important failure mechanism requiring accurate numerical models to implement simulations essential for failure prediction. To perform numerical simulation, the computational methods must be applied to determine fracture response and reliability of cracked structures. A current popular method is finite element (FEM), which has been extensively used for fracture analysis of cracks. Although a significant amount of the research in FEM is useful, the method has serious limitations in solving solid mechanics problems characterized by a continuous change in geometry of the domain under analysis. Crack propagation is a prime example in which the use of FEM requires a large number of remeshings of the finite element model to represent arbitrary and complex paths. The underlying structures of FEM and similar methods, which rely on a mesh, is quite cumbersome in treating cracks, that is not coincident with the original mesh geometry. Consequently, the only viable option for dealing with moving cracks model evolution so that mesh lines remain coincident with cracks throughout the analysis. This creates numerical difficulties, often leading to degradation of solution accuracy, complexity in computer programming, and a computationally intensive environment.

The principal attraction of meshless methods is possibility of simplifying adaptively and problems with moving boundaries and discontinuities, such as phase changes or cracks. In crack growth problems, for example, nodes can be added around a crack tip to capture the stress intensity factor with the desired accuracy; this nodal refinement can be moved with a propagating crack through a background arrangement of nodes associated with the global geometry. Adaptive meshing for a large variety of problems, including linear and non-linear stress analysis, can be effectively treated by these methods in a simple manner.

1.2 LITERATURE SURVEY

In the field of computational mechanics, extensive research has been done in the effective use of finite element method for problems in solid mechanics (fracture mechanics). Effort has been primarily focused on the modification of the approximation, incorporating the singularity present in the domain. The element free Galerkin method is a recently developed computational tool, which has been extensively for computing arbitrary crack paths. This class of methods is often called meshless, gridless or particle methods because of the absence of any predefined nodal connectivity.

In the past decades, for the solution of growing crack problems finite element methods with remeshing and boundary element methods is used but each has substantial disadvantages, which preclude their application to many important engineering problems. In the first one that involves a considerable amount of engineering effort and can result in substantial errors, it is almost impossible to automatically remesh finite elements about arbitrarily growing crack. Boundary element methods avoid a large part of the remeshing associated with finite element methods because only the surface of the crack, or in two dimensions, the line representation of the crack, needs to be remeshed. However, since boundary element methods require a Green function for the underlying partial differential equations, they are quite limited in the scope of problems they can attack.

Meshless method has been in existence since the late 1970's. Lucy (1977) introduced a particle method called smoothed particle hydrodynamics (SPH) for modeling astrophysical phenomena and in the 1980's Monaghan (1982) used this method for problems without boundaries, such as rotating stars and dust clouds and to solve the solid mechanics problems and further extended to solve the solid mechanics problems. In recent years, a class of meshfree or meshless methods, such as smooth particle hydrodynamics, diffuse element method, element free Galerkin method, *hp* clouds, partition of unity, reproducing kernel particle method, meshless local Petrov-Galerkin method and local boundary integral equation

method appear to demonstrate significant potential for the moving boundary problem like growing cracks. Fundamental to all mesh free methods, a structured mesh is not used, since only a scattered set of nodal points is required in the domain of interest.

Meshless methods based on partitions on unity seem to provide an efficient vehicle for performing hp adaptivity. These methods include hp-clouds and the partition of unity finite element method (PUFEM). The hp-clouds methods begins with a partition of unity based on moving least squares and enhances the polynomial order of the approximation through an extrinsic basis which can be added locally to nodes.

Other meshless methods, which have evolved, are the particle in cell (PIC) method, the generalized finite difference method and the finite point method. Belytschko (1996) provide a comprehensive review of the state-of-the-art in meshless methods and details the relationship between several of the key methods.

The essential idea of EFG methods is the use of moving least squares interpolants. Such interpolants were first described in a limited form by Shepard (1968): a more complete description can be found in the article by Lancaster and Salkauskas (1981). These interpolants were evidently independently discovered later who were the first to sue these in Galerkin methods: they called them diffuse elements and used these methods or the solution of heat conduction problems.

A formulation has been presented by Belytschko (1995) for consistently coupling EFG and FE by blending the approximations in a transition element. This allows the speed and simplicity of finite elements to be exploited where possible while allowing EFG to be used in regions where a meshless method is appropriate. But our problem of crack propagation for arbitrary paths is inherently difficult and also compromises the salient feature of EFGM. Jasiuk (1995) modeled fracture and crack growth with finite elements by deleting which met a yield criterion. This approach, which is not based on fracture mechanics, requires a very fine mesh to

get an acceptable representation of a crack. Other techniques for modeling crack growth include spring network models in which the material is represented by a network of spring and crack propagation is simulated by breaking spring Schlangen and Mier (1992).

The most obvious way to handle crack propagation is by remeshing the geometry. Swenson and Ingraffea (1988) presented a local remeshing technique in which elements ahead of the crack tip in the propagation direction were removed and the crack was extended. This area was triangulated to create a new local crack tip mesh. This method has the advantage that a vast amount of existing finite element technology can be used for support. There are some drawbacks to this method such as difficulties if the crack step size is too small, then remeshing is unwarranted. Complex geometries and interacting crack tip are also potential difficulties as is rerunning a step with a smaller crack increment.

1.3 Thesis organization

This thesis is focus on the element free Galerkin (EFG) methods for computational fracture mechanics and is organized as follows:

In chapter 2, we briefly review of linear elastic fracture mechanics and introduce the J integral for numerically computing stress intensity factors. Quasi-static fracture crack is discussed and algorithm for their simulation by element free Galerkin (EFG) are introduced.

In chapter 3, the moving least square methodology is reviewed and used to construct discrete EFG approximation. The elastic static boundary value problem is presented along with its associated weak form. Approximation of the solution with EFG is presented and topics of nodal domains of influence and integration of weak form are discussed. It should be noted that the definition of a meshless method is one in which no predefined element connectivity exists for determining the approximant. Some confusion invarbly arises when the meshless approximant is used in Galerkin method. Integration of weak form is performed by Gauss

quardrature, which requires some sort of integration cells. Although this detracts from the meshless nature of the method the background cell structure by no means destroys it. Smoothing of EFG approximation near nonconvex boundaries is presented. Without smoothing, EFG approximation near nonconvex boundaries such as crack tips will contain discontinuities, which extend into the domain. These discontinuities arise due to a sampling point grazes the boundary. The diffraction method smoothes EFG approximation by wrapping the nodal support a short distance around the point at which the discontinuity would begin.

In chapter 4, several example problems are presented to illustrate the effectiveness of EFG for solving problem of arbitrary crack growth.

Finally in chapter 5, the work is summarized and the relevant conclusions and the scope of the future work were presented.

CHAPTER 2

LINEAR ELASTIC FRACURE MECHANICS

2.1 Parameterization of fracture field

The presence of a crack has a considerable effect on the stress field and load bearing capacity of a body. For cracks in linear elastic media, the stress fields are well known and can be expressed in terms of parameters, which include the effects of crack length, applied loads, and other conditions such as boundary effects. The two parameters, which will be discussed, are the stress intensity factor and the energy release rate. The stress intensity factor is a local crack tip parameter, which describes the stress field at a crack tip, while the energy release rate is a global parameter, which gives the change in elastic energy for an infinitesimal crack advance.

Fracture modes

The displacement field around a crack can be categorized by the three modes shown in Fig 2.1. Mode I is called the *opening mode* and is charactized by displacements of the crack normal to the plane of the crack. Mode II is called the *shearing or sliding mode* and is characterized by in-plane displacements of the crack faces parallel to the crack surface. Mode III is called the *tearing or antiplane mode* and is characterized by shear deformation out of the plane of the crack.

In this report, only two dimensional plane problems are presented and hence mode I and mode II fracture are considered.

Stress intensity factors

The stress at the tip of a linear elastic crack is $1/\sqrt{r}$ singular, where r is the distance from the crack tip. The stress field near the crack tip is dominated by the first term in the asymptotic. For a mode I crack (displacement perpendicular to the crack faces), the stresses can be written as

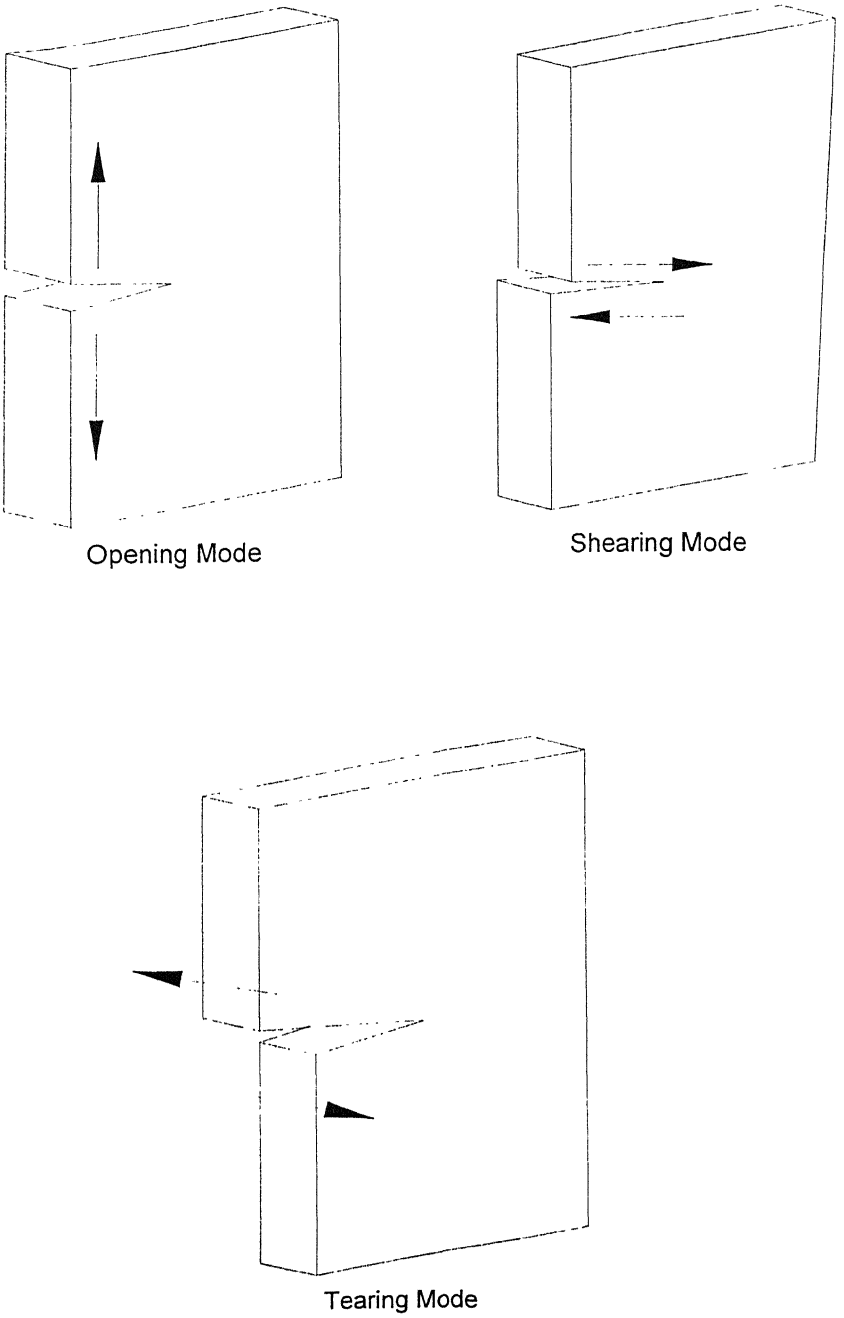

Fig. 2.1 Schematic drawing of the three fracture modes

$$\sigma_{xx} = \frac{K_I}{\sqrt{2\pi r}} \cos\frac{\theta}{2}\left(1 - \sin\frac{\theta}{2}\sin\frac{3\theta}{2}\right) \quad \ldots (2.01)$$

$$\sigma_{yy} = \frac{K_I}{\sqrt{2\pi r}} \cos\frac{\theta}{2}\left(1 + \sin\frac{\theta}{2}\sin\frac{3\theta}{2}\right) \quad \ldots (2.02)$$

$$\sigma_{xy} = \frac{K_I}{\sqrt{2\pi r}} \cos\frac{\theta}{2}\sin\frac{\theta}{2}\sin\frac{3\theta}{2} \quad \ldots (2.03)$$

The associated compatible displacement field is

$$u_x = \frac{K_I}{2\mu}\sqrt{\frac{r}{2\pi}} \cos\frac{\theta}{2}\left(\kappa - 1 + 2\sin^2\frac{\theta}{2}\right) \quad \ldots (2.04)$$

$$u_y = \frac{K_I}{2\mu}\sqrt{\frac{r}{2\pi}} \sin\frac{\theta}{2}\left(\kappa + 1 - 2\cos^2\frac{\theta}{2}\right) \quad \ldots (2.05)$$

For a mode II crack (displacement parallel to crack faces) the stresses can be written

$$\sigma_{xx} = \frac{K_{II}}{\sqrt{2\pi r}} \cos\frac{\theta}{2}\left[-\sin\frac{\theta}{2}\left(2 + \cos\frac{\theta}{2}\cos\frac{3\theta}{2}\right)\right] \quad \ldots (2.06)$$

$$\sigma_{yy} = \frac{K_{II}}{\sqrt{2\pi r}} \cos\frac{\theta}{2}\left(1 + \sin\frac{\theta}{2}\sin\frac{3\theta}{2}\right) \quad \ldots (2.07)$$

$$\sigma_{xy} = \frac{K_{II}}{\sqrt{2\pi r}} \cos\frac{\theta}{2}\left[\cos\frac{\theta}{2}\left(1 - \sin\frac{\theta}{2}\sin\frac{3\theta}{2}\right)\right] \quad \ldots (2.08)$$

With the associated displacement field

$$u_x = \frac{K_{II}}{2\mu}\sqrt{\frac{r}{2\pi}} \sin\frac{\theta}{2}\left(\kappa + 1 + 2\cos^2\frac{\theta}{2}\right) \quad \ldots (2.09)$$

$$u_y = \frac{K_{II}}{2\mu}\sqrt{\frac{r}{2\pi}}\left(-\cos\frac{\theta}{2}\right)\left(\kappa - 1 - 2\sin^2\frac{\theta}{2}\right) \quad \ldots (2.10)$$

The variables r and θ are the radius from the crack tip and the angle measured from the line ahead of the crack, respectively (see Fig. 2.2) is the Kolosov constant κ written in terms of Poisson's ratio υ.

$$\kappa = \begin{cases} 3-4\upsilon & plane\ \ strain \\ \dfrac{3-\upsilon}{1+\upsilon} & plane\ \ stress \end{cases}$$

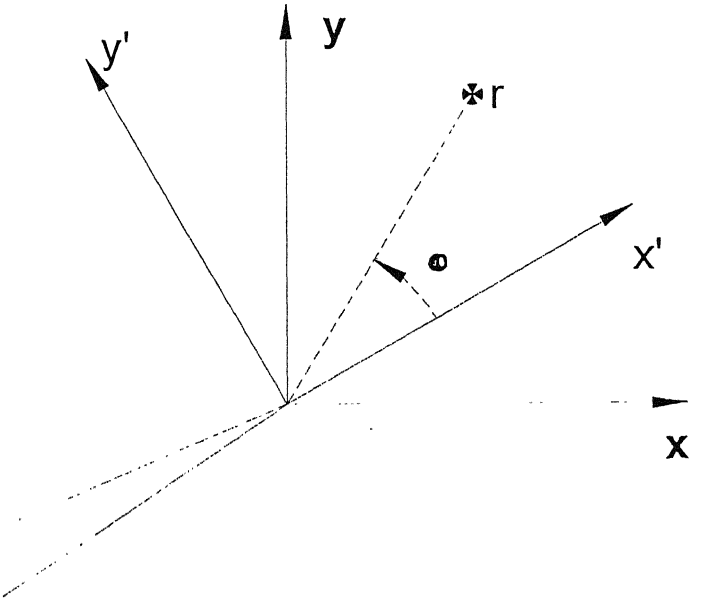

Fig. 2.2 Local coordinate system at crack tip.

The mode I and mode II stress intensity factors, K_I and K_{II} are constants, which depend on the crack length, specimen geometry and applied loading. It is significant to note that determination of these constants completely determines the asymptotic stress and displacement fields around the crack tip.

In case where the loading and geometry give a combination of *opening* (mode I) and *shearing* (mode II) displacements, the stress field will be a combination of previous equations. In polar coordinates, the crack tip stresses are

$$\sigma_{rr} = \frac{1}{\sqrt{2\pi r}} \cos\frac{\theta}{2}\left[K_I \left(1+\sin^2\frac{\theta}{2}\right) + K_{II}\left(\frac{3}{2}\sin\frac{\theta}{2} - 2\tan\frac{\theta}{2}\right)\right] \quad \ldots . (2.11)$$

$$\sigma_{\theta\theta} = \frac{1}{\sqrt{2\pi r}} \cos\frac{\theta}{2}\left[K_I \cos^2\frac{\theta}{2} - \frac{3}{2} K_{II} \sin\theta \right] \quad \ldots . (2.12)$$

$$\sigma_{r\theta} = \frac{1}{\sqrt{2\pi r}} \cos\frac{\theta}{2}\left[\frac{1}{2} K_I \sin\theta + \frac{1}{2} K_{II}(3\cos\theta - 1)\right] \quad \ldots . (2.13)$$

2.2 Computation of fracture parameters

A great deal of research has gone into methods of determining stress intensity factor for various geometries and loadings. The developments of numerical methods such as finite elements and boundary elements have facilitated the calculation of crack tip stress fields and many methods have been developed for inferring stress intensity factor (e.g., displacement and stress extrapolation, displacement and stress correlation, enriched elements, *J* integral). The *J* integral is popular because of its robustness as well as adaptability to mixed mode problems.

J integral

The *J* integral is given by

$$J = \int_{\Gamma} \left[W\delta_{1j} - \sigma_{ij} \frac{\partial u_i}{\partial x_1} \right] n_j d\Gamma \quad \ldots . (2.14)$$

where $W = \int_0^{\varepsilon} \sigma d\varepsilon$ is the strain energy density, σ is the Cauchy stress, and n is the outward unit normal to an arbitrary contour enclosing the crack tip. The path independence property allows the *J* integral to be evaluated using far field

information, which is generally more accurate, that near-tip results for numerical methods. Path independence is easily shown by considering the closed contour

$\Gamma = \Gamma_1 + C_+ + \Gamma_2 + C_-$ Around the tip of a straight crack with **m** as the normal to the closed contour. Along the entire contour previous can be written

$$J' = \int_{\Gamma_1} \left[W\delta_{1j} - \sigma_{ij} \frac{\partial u_i}{\partial x_1} \right] m_j d\Gamma + \int_{\Gamma_2} \left[W\delta_{1j} - \sigma_{ij} \frac{\partial u_i}{\partial x_1} \right] m_j d\Gamma + \int_{C_+ + C_-} \left[Wn_1 - \sigma_{ij} \frac{\partial u_i}{\partial x_1} \right] m_j d\Gamma = 0 \quad \ldots . (2.15)$$

where the prime is used to indicate that J is written for a closed contour. Along the crack faces C+C-, $m_1 = 0$ and $\sigma_{ij} m_j = t_i = 0$ (traction free crack faces) so that the last integral equation is zero. Reversing the direction of the normal m on the inside contour Γ_1 to be the outward normal n_{Γ_1} leads to $J_{\Gamma_1} = J_{\Gamma_2}$.

Domain form of *J* integral

The contour integral equation can be converted into equivalent form to enhance the usefulness of the *J* integral in certain cases. The evaluation of contour integrals is difficult with finite elements because the stress field is discontinuous and performing an area integral is more convenient.

Consider a closed contour with weight function ***q*** included in the integeral and

$$J = \int_{\Gamma_1} \left[W\delta_{1j} - \sigma_{ij} \frac{\partial u_i}{\partial x_1} \right] m_j q d\Gamma \quad \ldots . (2.16)$$

Here, *m* is the outward normal to the closed contour Γ and the prime denotes a closed contour for *J*. The weight function q is defined so that

$$q = \begin{cases} 1 & on & \Gamma_1 \\ 0 & on & \Gamma_2 \\ arbitrary & other & wise \end{cases}$$

Since q=0 on Γ_2 and the integer and vanishes on C_+ and C_-, the closed contour integral is reduces to a closed integral on Γ_1

$$J = \int_{\Gamma_1} \left[W\delta_{1j} - \sigma_{ij} \frac{\partial u_i}{\partial x_1} \right] m_j d\Gamma \qquad \ldots . (2.17)$$

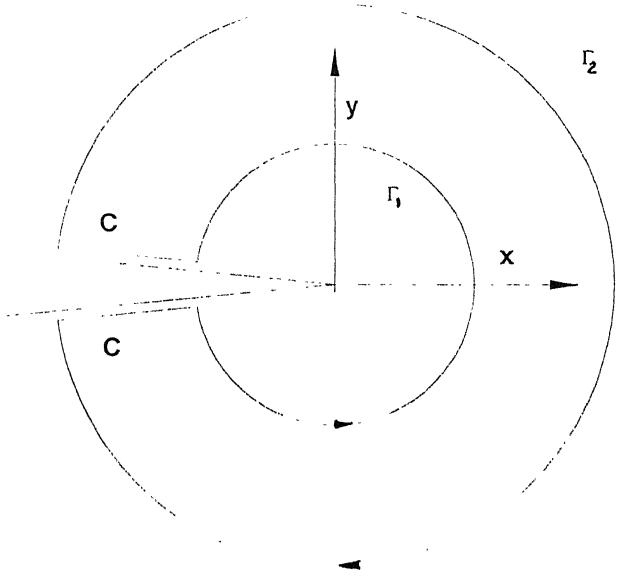

Fig. 2.3 Path Independent closed contour about the tip of a crack

Applying the divergence theorem to obtain the area integral

$$J' = \int_A \left[\frac{\partial}{\partial x_j} \left[W\delta_{1j} - \sigma_{ij} \frac{du_i}{dx_1} \right] q + \left[W\delta_{1j} - \sigma_{ij} \frac{du_i}{dx_1} \right] \frac{\partial q}{\partial x_j} \right] dA \qquad \ldots . (2.18)$$

For linear elasticity, the first term is vanishes. Comparing both equation and reversing the normal *m* in the equation to be outward normal n_{Γ_1} leads to

$$\int_{\Gamma_1} \left[W\delta_{1j} - \sigma_{ij} \frac{\partial u_i}{\partial x_1} \right] n_j d\Gamma = \int_A \left[\sigma_{ij} \frac{\partial u_i}{\partial x_1} - W\delta_{1j} \right] \frac{\partial q}{\partial x_j} dA \qquad \ldots . (2.19)$$

The domain form of the J integral is then

$$J = \int_A \left[\sigma_{ij} \frac{\partial u_i}{\partial x_1} - W\delta_{1j} \right] \frac{\partial q}{\partial x_j} dA \qquad \ldots . (2.20)$$

Interaction integral

The J integral defined in equation is equal to the energy release rate for elastic materials. For a general mixed-mode case

$$J = G = \frac{1}{E'} \left(\mathrm{K}_{\mathrm{I}}^2 + \mathrm{K}_{\mathrm{II}}^2 \right) \qquad \ldots . (2.21)$$

where

$$E' = \begin{cases} E & plane \quad stress \\ \dfrac{E}{1-\nu^2} & plane \quad strain \end{cases}$$

The individual stress intensity factors K_{I} and K_{II} are needed to compute the direction and growth of fracture crack.

Considering two independent equilibrium states of a cracked body, where state 1 is defined here to be the actual state for the given boundary conditions while state 2 is defined to be an auxiliary state, which will be given later. The J integral for the two superposed states is

$$J^{tot} = \int_\Gamma \left[W^{tot}\delta_{1j} - \left(\sigma_{ij}^{(1)} + \sigma_{ij}^{(2)} \right) \frac{\partial \left(u_i^{(1)} + u_i^{(2)} \right)}{\partial x_1} \right] n_j d\Gamma \qquad \ldots . (2.22)$$

where

$$W^{tot} = \frac{1}{2} \left(\sigma_{ij}^{(1)} + \sigma_{ij}^{(2)} \right) \left(\varepsilon_{ij}^{(1)} + \varepsilon_{ij}^{(2)} \right) \qquad \ldots . (2.23)$$

The upper equation can be rearranged to yield

$$J^{tot} = \int_{\Gamma} \left[W^{(1)}\delta_{1j} - \sigma_{ij}{}^{(1)} \frac{\partial u_i{}^{(1)}}{\partial x_1} \right] n_j d\Gamma + \int_{\Gamma} \left[W^{(2)}\delta_{1j} - \sigma_{ij}{}^{(2)} \frac{\partial u_i{}^{(2)}}{\partial x_1} \right] n_j d\Gamma$$
$$+ \int_{\Gamma} \left[W^{(1,2)}\delta_{1j} - \sigma_{ij}{}^{(1)} \frac{\partial u_i{}^{(2)}}{\partial x_1} - \sigma_{ij}{}^{(2)} \frac{\partial u_i{}^{(1)}}{\partial x_2} \right] n_j d\Gamma$$

. . . . (2.24)

$$J^{tot} = J^{(1)} + J^{(2)} + M^{(1,2)} \qquad \text{. . . . (2.25)}$$

where $J^{(1)}$ and $J^{(2)}$ are the J integrals for state 1 and state 2, respectively. $M^{(1,2)}$ is the interaction integral for the two equilibrium states.

$$M^{(1,2)} = \int_{\Gamma} \left[W^{(1,2)}\delta_{1j} - \sigma_{ij}{}^{(1)} \frac{\partial u^{(2)}}{\partial x_1} - \sigma_{ij}{}^{(2)} \frac{\partial u_i{}^{(1)}}{\partial x_1} \right] n_j d\Gamma \qquad \text{. . . . (2.26)}$$

and $W^{(1,2)}$ is the mutual strain energy

$$W^{(1,2)} = \frac{1}{2}\left(\sigma_{ij}{}^{(1)} \varepsilon_{ij}{}^{(2)} + \sigma_{ij}{}^{(2)} \varepsilon_{ij}{}^{(1)} \right) \qquad \text{. . . . (2.27)}$$

$$W^{(1,2)} = \sigma_{ij}{}^{(1)} \varepsilon_{ij}{}^{(2)} = \sigma_{ij}{}^{(2)} \varepsilon_{ij}{}^{(1)} \qquad \text{. . . . (2.28)}$$

From the Irwin's relation fro the superposed states is written

$$J^{tot} = \frac{2}{E'}\left[\left(\left(K_I{}^{(1)} \right)^2 + \left(K_{II}{}^{(1)} \right)^2 \right) + \left(\left(K_I{}^{(2)} \right)^2 + \left(K_{II}{}^{(2)} \right)^2 \right) + \left(K_I{}^{(1)} K_I{}^{(2)} + K_{II}{}^{(1)} K_{II}{}^{(2)} \right) \right] \qquad (2.29)$$

$$J^{tot} = J^{(1)} + J^{(2)} + \frac{2}{E'}\left(K_I{}^{(1)} K_I{}^{(2)} + K_{II}{}^{(1)} K_{II}{}^{(2)} \right) \qquad \text{. . . . (2.30)}$$

So comparing of the equations leads to relationship

$$M^{(1,2)} = \frac{2}{E'}\left(K_I{}^{(1)} K_I{}^{(2)} + K_{II}{}^{(1)} K_{II}{}^{(2)} \right) \qquad \text{. . . . (2.31)}$$

Obtaining the individual stress intensity factors from the actual field requires

that the auxiliary field be chosen judiciously. For the case, $K_I^{(2)} = 1, K_{II}^{(2)} = 0$ earlier equations reduce to $M^{(1,2)} = \frac{2}{E'} K_I^{(1)}$.

Similarly, the mode II stress intensity factor can be found with $K_I^{(2)} = 0, K_{II}^{(2)} = 1$ equation is reduces to $M^{(1,2)} = \frac{2}{E'} K_{II}^{(2)}$

Thus, the contour integral can be converted to an equivalent domain integral by Gauss's theorem and leads to the equation

$$M^{(1,2)} = \int_A \left[\sigma_{ij}^{(1)} \frac{\partial u_i^{(2)}}{\partial x_1} + \sigma_{ij}^{(2)} \frac{\partial u_i^{(1)}}{\partial x_1} - W^{(1,2)} \delta_{1j} \right] \frac{\partial q}{\partial x_j} dA \quad \ldots . (2.32)$$

It should be noted that interaction integral as described is only valid for elastic materials because of the auxiliary field chosen. However, the stress intensity factor as a fracture parameter is only valid when crack tip plasticity is negligible and so this limitation on the interaction integral should not be of concern.

2.3 Crack growth direction

Modeling crack propagation requires a law for the direction of crack growth. The most commonly used laws are

1. The maximum principal stress criterion

2. The maximum energy release rate criterion

3. The minimum strain energy density criterion

The first two criteria have been identical for the electrostatic fracture, although they are not necessarily the same for dynamic fracture. The minimum strain energy density criterion assumes that the strain energy density near crack tip is a quadratic function of mode I and mode II stress intensity factors. Crack extension is assumed to occur in the direction, which minimizes the strain energy

density. In this report, the maximum principal stress criterion is used for computing the direction of crack extension.

The maximum principal stress criterion states that a crack will grow in a direction perpendicular to the maximum hoop stress, $\sigma_{\theta\theta}$. For a general mixed-mode state of stress, the stresses at the crack tip are given by the earlier equation. The direction of maximum hoop stress is the orientation in which the shear stress vanishes

$$\sigma_{r\theta} = \frac{1}{\sqrt{2\pi r}}\cos\frac{\theta}{2}\left[\frac{1}{2}\mathrm{K_I}\sin\frac{\theta}{2} + \frac{1}{2}\mathrm{K_{II}}(3\cos\theta - 1)\right] \quad \ldots . (2.33)$$

The solution $\cos\frac{\theta}{2} = 0$ yields an angle $\theta = \pm 180°$, which is ignored because it is irrelevant. The other solution is obtained by setting the term in the square brackets to zero. This leads to the condition

$$\mathrm{K_I}\sin\theta_m + \mathrm{K_{II}}(3\cos\theta_m - 1) = 0 \quad \ldots . (2.34)$$

which must be solved for the angle of crack propagation, θ_m.

For this angle, $\sigma_{\theta\theta}$ is principal stress field. This means that $\sigma_{\theta\theta}$ may be written in terms of an equivalent mode I stress intensity factor instead of the mixed mode stress intensity factors, which leads to

$$\sigma_{\theta\theta} = \frac{1}{\sqrt{2\pi r}}\cos\frac{\theta_m}{2}\left[\mathrm{K_I}\cos^2\frac{\theta_m}{2} - \frac{3}{2}\mathrm{K_{II}}\sin\theta_m\right] = \frac{\mathrm{K_{Ieq}}}{\sqrt{2\pi r}} \quad \ldots . (2.35)$$

where

$$\mathrm{K_{Ieq}} = \mathrm{K_I}\cos^3\frac{\theta_m}{2} - 3\mathrm{K_{II}}\cos^2\frac{\theta_m}{2}\sin\frac{\theta_m}{2} \quad \ldots . (2.36)$$

The equivalent mode I stress intensity factor, $\mathrm{K_{Ieq}}$, provides a single measure of the mixed-mode stress field and is used in crack growth laws for computing the crack growth rate mixed-mode loading.

Multiple cracks

The crack growth methodology presented in the previous section requires some modification if more than one crack is present and growing. The stress field at the tip of each crack will be different and thus some cracks will grow faster than others and some may not grow at all.

Algorithm used for growing multiple quasi-static crack

1.compute the stress field

2.compute stress intensity factors for each crack

Compute incipient crack growth angle θ_m using maximum principal stress criterion

#Compute equivalent mode I stress intensity factor K_{Ieq}

3.find crack with highest K_{Ieq}, i.e. fastest growing crack

Set $\Delta a = \Delta a_{\max}$ for this crack

4.compute the crack increment for each based on $\Delta a = \Delta a_{\max}\left(\frac{K_{Ieq}}{K_{Ieq}^{\max}}\right)^2$

Note: if $K_{Ieq} < K_c$ for a crack, then $\Delta a = 0$ for that crack

5.increment each crack

6.if another step of crack growth is desired, go to step 1

7.end analysis

Quasi-static crack propagation

Quasi-static fracture refers to crack propagation at or above the fracture toughness. No accepted standard for computing the crack growth rate exists in this condition, and the crack is assumed to propagate as long as the stress intensity factor is greater than the fracture toughness, i.e. whenever $K \geq K_{IC}$ is satisfied.

Crack growth may be classified as stable and unstable based on the change in stress intensity factor with growth. In stable fracture, the stress intensity factor decreases as the crack propagates and crack will eventually arrest when it falls below the fracture toughness. Examples of stable fracture are cracked specimens loaded by prescribed displacement and cracks in an overall compressive field. In unstable fracture, the stress intensity factor increases with crack length and propagating crack never arrests.

Fracture stability is easily understood by considering a compact tension specimen with a prescribed displacement and prescribed load. For the prescribed load, the stress intensity factor continues to increase as the crack extends, indicating unstable fracture. For the prescribed displacement, the stress intensity factor decrease as the crack grows and eventually falls below the fracture toughness. The crack arrests at this point.

2.4 Closure

In this chapter briefly review of linear elastic fracture mechanics and introduce the J integral for numerically computing stress intensity factors. Quasi-static fracture crack is discussed and algorithm for their simulation by element free Galerkin (EFG) are introduced.

CHAPTER 3

ELEMENT FREE GALERKIN METHOD

3.1 Introduction

The element-free Galerkin (EFG) method is a meshless method because only a set of nodes is required to generate the discrete equations. The connectivity between the nodes and the approximation functions are completely constructed by the method.

The EFG method employs moving least-square (MLS) approximants to approximate the function $u(x)$ with $u^h(x)$ Belytschko,(1998).The approximation of $u^h(x)$ the function $u(x)$ at any point x in the problem domain Ω is written $u^h(x) = p^T(x)a(x)$. These approximants are constructed from three components: a weight function of compact support associated with each node; a basis, usually consisting of a polynomial; and a set of coefficients that depend on position. The weight function is nonzero only over a small sub domain around a node, which is called its support. The support of the weight function defines a node's domain of influence, which is the sub domain over which a particular node contributes to the approximation. The overlap of nodal domains of influence defines the nodal connectivity.

One attractive property of MLS approximants is that their continuity is related to the continuity of the weight function, if the continuity of the basis is greater than the continuity of the weight function, the resulting approximation will inherit the continuity of the weight function. Therefore, a low order polynomial basis, e.g., a linear basis, may be used to generate a higher order continuous approximations by choosing an appropriate weight function. Thus, post processing stress and strain results to generate smooth fields that is required for finite element methods is unnecessary in EFG.

Although EFG is considered meshless with reference to shape function construction or function approximation, a mesh will be required for solving partial differential equations (PDE's) by Galerkin approximation procedure. In order to compute the integrals in the weak form, either a regular background mesh or a background cell structure is used.

3.2 Meshless approximations by MLS

The approximation of $u^h(x)$ the function $u(x)$ at any point x in the problem domain Ω is written

$$u^h(x) = p^T(x)a(x) \qquad \ldots\ldots (3.1)$$

where $p(x)$ is a basis (usually polynomial) and $a(x)$ are unknown coefficients. Some complete polynomial basis is

1D: $p^T(x) = [1, x]$ linear. $\ldots\ldots$ (3.2 a)

$p^T(x) = [1, x, x^2]$ quadratic. $\ldots\ldots$ (3.2 b)

2D: $p^T(x) = [1, x, y]$ linear. $\ldots\ldots$ (3.3 c)

$p^T(x) = [1, x, y, x^2, xy, y^2]$ quadratic. $\ldots\ldots$ (3.2 d)

Sometime some other function can be added to the basis in situations where it is desirable to enrich the solution.

To find field variable by earlier equation, it is necessary to determine the coefficients $a(x)$. The moving least squares (MLS) methodology [Lancaster and Salkauskas, 1981] is an effective technique for approximating a function using a set of scattered data. Given a set of nodes with coordinates x_I at which the field variable u_I is known, weighted norm L_2 can be written

$$J(x)=\sum_{I=1}^{n} w(x-x_I)\left[p^T(x_I)a(x)-u_I\right]^2 \qquad \ldots\ldots (3.3)$$

where $w(x-x_I)$ is the weight function of node I at point x, and n is the number of neighbours of point x, i.e., nodes with $w(x-x_I)>0$ and u_I refers to the nodal parameter of u at $x=x_I$ Note that $u^h(x_I)\neq u_I$. This neighborhood Ω_I is called the domain of influence of x, or circle of influence in two dimensions. The domain of influence of a point is shown in Fig.3.1.

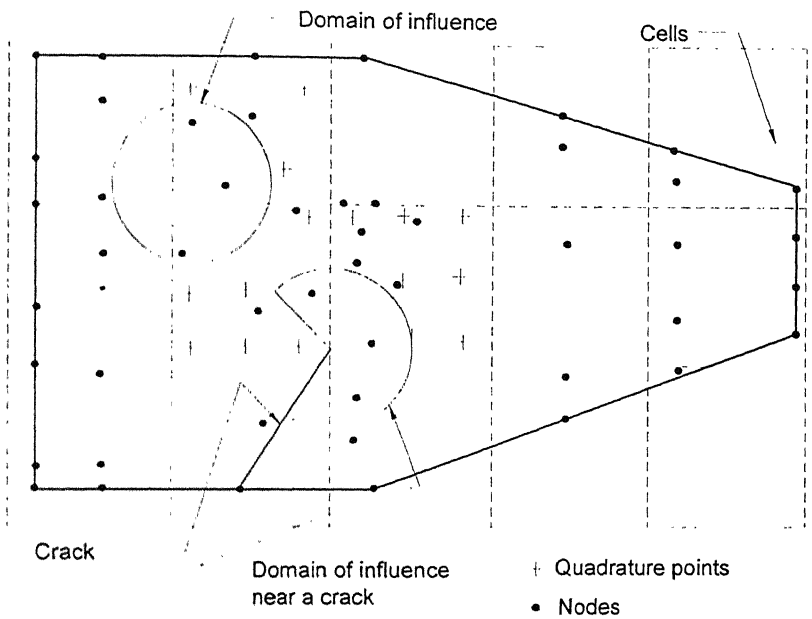

Fig. 3.1 Cell structure used for the integration for EFG and domain of influence around the quadrature points.

Finding the minimum of $J(x)$ with respect to $a(x)$ leads to a set of linear equations

$$A(x)a(x)=C(x)u \qquad \ldots\ldots (3.4)$$

For example, for linear approximation,

$$A(x)=\sum_{I=1}^{n} w(x-x_I)p(x_I)p^T(x_I) \qquad \ldots\ldots (3.5)$$

$$= w(x-x_I)\begin{bmatrix} 1 & x_1 & y_1 \\ x_1 & x_1^{\,2} & x_1y_1 \\ y_1 & x_1y_1 & y_1^{\,2} \end{bmatrix} + w(x-x_2)\begin{bmatrix} 1 & x_2 & y_2 \\ x_2 & x_2^{\,2} & x_2y_2 \\ y_2 & x_2y_2 & y_2^{\,2} \end{bmatrix} + \cdots w(x-x_n)\begin{bmatrix} 1 & x_n & y_n \\ x_n & x_n^{\,2} & x_ny_n \\ y_n & x_ny_n & y_n^{\,2} \end{bmatrix} \qquad \ldots\ldots (3.6)$$

$$C(x)=[w(x-x_I)p(x_I), w(x-x_2)p(x_2),\ldots. w(x-x_n)p(x_n)] \qquad \ldots\ldots (3.7)$$

$$= \left[w(x-x_1)\begin{bmatrix} 1 \\ x_1 \\ y_1 \end{bmatrix} \cdot w(x-x_2)\begin{bmatrix} 1 \\ x_2 \\ y_2 \end{bmatrix} \cdots w(x-x_n)\begin{bmatrix} 1 \\ x_n \\ y_n \end{bmatrix} \right]$$

$$u=[u_1, u_2, \ldots. u_n] \qquad \ldots\ldots (3.8)$$

The matrix $A(x)$ is often called the moment matrix and $C(x)$ is a matrix of column vectors. So eq. 3.4 can be solved for $a(x)$ to yield

$$a(x)=A^{-1}(x)C(x)u \qquad \ldots\ldots (3.9)$$

which can be substituted into eq. 3.1 to yield an approximation in terms of the nodal coefficients

$$u^h(x)=\sum_{I=1}^{n} p^T(x)A^{-1}(x)C_I(x)u_I \qquad \ldots\ldots (3.10)$$

where $C_I(x)$ is the Ith column of $C(x)$ and u_I is the nodal coefficient for the Ith neighbor of x. Defining the shape function as $\phi_I(x)=p^T(x)A^{-1}(x)C_I(x)$

Allows the approximation to be written as

$$u^h(x) = \sum_{I=1}^{n} \phi_I(x) u_I \qquad \ldots\ldots (3.11)$$

which is a form similar to those in the finite element method.

It should be noted that these shape functions do not satisfy the condition

$$\phi_I(x_J) \neq \delta_{IJ} \qquad \ldots\ldots (3.12)$$

where δ_{IJ} is the Kronecker delta. In the finite element method, where is equation of essential boundary conditions can easily be applied, imposing essential boundary conditions is difficult in the EFG method. In the EFG method the displacement at a point x_J on the boundary node is given by

$$u(x_J) = \sum_{I=1}^{n} \phi_I(x_J) u_I \qquad \ldots\ldots (3.13)$$

where $I = 1$ to n are all nodes in the domain of influence of x_J; because of $u(x_I) \neq u_I$, so setting $u_I = 0$ on the boundary does not ensure that $u(x) = 0$ on the boundary.

To determine the derivative form the displacement; it is necessary to obtain the shape function. The spatial derivatives of the shape functions, computed by the chain rule, are

$$\phi_{I,i}(x) = p^T{}_{,i}(x) A^{-1}(x) C_I(x) + p^T(x)\left[A^{-1}{}_{,i}(x) C_I(x) + A^{-1}(x) C_{I,i}(x)\right]. \qquad \ldots\ldots (3.14)$$

where $A^{-1}{}_{,i} = -A^{-1} A_{,i} A^{-1}$ note that the second term in equation is expensive to compute because of the term $A_{,i}^{-1}$.

3.3 Shape Function And Its Derivatives

To compute the shape functions from the previous equation it is necessary to invert the A matrix. In one dimension, this operation is not computationally expensive, but in two or three dimensions it becomes quite difficult. An alternative approach that is much more computationally efficient was proposed by *Belystchko al (1996)*. This method involves the LU decomposition of the A matrix.

The shape function is equation can be written as

$$\phi_I(x) = p^T(x)A^{-1}(x)C_I(x)$$

$$= \gamma^T(x)C_I(x) \qquad \ldots\ldots (3.15)$$

with corresponding derivatives

$$\phi_{I,i}(x) = \gamma^T{}_{,i}(x)C_I(x) + \gamma^T(x)C_{I,i}(x) \qquad \ldots\ldots (3.16)$$

Comparing the terms of eq. 3.15 leads to the relationship

$$A(x)\gamma(x) = p(x) \qquad \ldots\ldots (3.17)$$

The coefficients $\gamma(x)$ can be obtained by an LU decomposition of $A(x)$ and back substitution. This requires fewer computations than a full inversion of $A(x)$, which is required to form the shape functions with equation of $\phi_I(x)$.

The derivatives of $\gamma(x)$ is required to compute the shape function derivatives in equation $\phi_{I,i}(x)$. Taking the derivatives of eq. 3.17.

$$A_{,i}(x)\gamma(x) + A(x)\gamma_{,i}(x) = p_{,i}(x) \qquad \ldots\ldots (3.18)$$

and rearranging known terms of the above equation will be,

$$A(x)\gamma_{,i}(x) = p_{,i}(x) - A_{,i}(x)\gamma(x) \qquad \ldots\ldots (3.19)$$

Using the LU decomposition of $A(x)$, which is known from the solving equation, $\gamma_{,i}(x)$ can be computed with only a back substitution. Higher order derivatives can be easily obtained by repeating the procedure used for computing the first derivative.

3.4 Variational Function And Discretization

In two-dimensional, the equilibrium equations and boundary conditions are

$$\nabla \cdot \sigma + b = 0 \qquad \text{in } \Omega \qquad \ldots\ldots (3.20)$$

$$\sigma \cdot n = \bar{t} \qquad \text{on } \Gamma_t \text{ (traction boundary conditions)}$$

$$u = \bar{u} \qquad \text{on } \Gamma_u \text{ (essential boundary conditions)}$$

In which the superposed bar denotes prescribed boundary values, and n is the unit normal to the domain Ω. Here $\sigma = D\varepsilon$ is the stress vector, D is the material property matrix, $\varepsilon = \nabla_s u$ is the strain vector, ∇_s is the symmetric part of the gradient operator, u is the displacement vector, b is the body force vector, $\bar{t}$ and $\bar{u}$ are the vectors of prescribed surface tractions and displacements, respectively, n is a unit normal to domain, Ω, Γ_t and Γ_u are the portions of boundary, Γ where tractions and displacements are prescribed, respectively.

The variational (or weak) form for equilibrium equation can be written

$$\delta W = \int_\Omega \nabla_s \delta u : \sigma d\Omega - \int_\Omega \delta u \cdot b d\Omega - \int_{t_t} \delta u \cdot \bar{t} d\Gamma - \delta W_u(u) = 0 \quad (3.21)$$

The term $\delta W_u(u)$ is an additional term to account for essential boundary conditions in a meshless method and will be discussed in the subsequent part.

The term $\delta W_u(u)$ is necessary because, in contrast to finite-element methods, $\phi_I(x_J) \neq \delta_{IJ}$, so it is not sufficient to set the nodal displacements to

enforce essential boundary conditions. Several forms of $\delta W_u(u)$ are possible. In this work Lagrange multipliers are used, so

$$\delta W_u = \int_{\Gamma_u} \delta\lambda \cdot (u - \bar{u}) d\Gamma + \int_{\Gamma_u} \delta u \cdot \lambda d\Gamma \quad \ldots\ldots (3.22)$$

For linear elasticity

$$\varepsilon = \nabla_s u \quad \ldots\ldots (3.23)$$

which can be used to write the weak form from variational form equation in terms of the displacement u.

The discrete form of variational equation for a meshless method can be obtained by using the approximation form equation as an approximation for u and δu to get the system of equations

$$\mathrm{K}u = f^{ext} \quad \ldots\ldots (3.24)$$

The stiffness matrix K and the external force vector f^{ext} are composed of the sub matrices

$$\mathrm{K}_{IJ} = \int_{\Omega} B_I D B_J d\Omega \quad \ldots\ldots (3.25)$$

$$f_I^{ext} = \int_{\Gamma_t} \phi_I t d\Gamma + \int_{\Omega} \phi_I b d\Omega \quad \ldots\ldots (3.26)$$

where D is the constitutive matrix given by

$$D = \frac{E}{(1+\upsilon)(1-2\upsilon)} \begin{bmatrix} 1-\upsilon & \upsilon & 0 \\ \upsilon & 1-\upsilon & 0 \\ 0 & 0 & \frac{1-2\upsilon}{2} \end{bmatrix} \quad \text{plane strain}$$

$$D = \frac{E}{1-\upsilon^2}\begin{bmatrix} 1 & \upsilon & 0 \\ \upsilon & 1 & 0 \\ 0 & 0 & \frac{1-\upsilon}{2} \end{bmatrix}$$ plane stress

and B_i is a matrix of shape function derivatives

$$B_I = \begin{bmatrix} \phi_{I,x} & 0 \\ 0 & \phi_{I,y} \\ \phi_{I,y} & \phi_{I,x} \end{bmatrix}$$

3.5 Weight Function

Weight function are defined to be smooth and monotonically decreasing at each node such that the whole domain is covered. Common shapes of weight functions in two dimensions are circles and rectangles (see Fig.3.2). The counterparts of these in three dimensions are spheres and bricks.

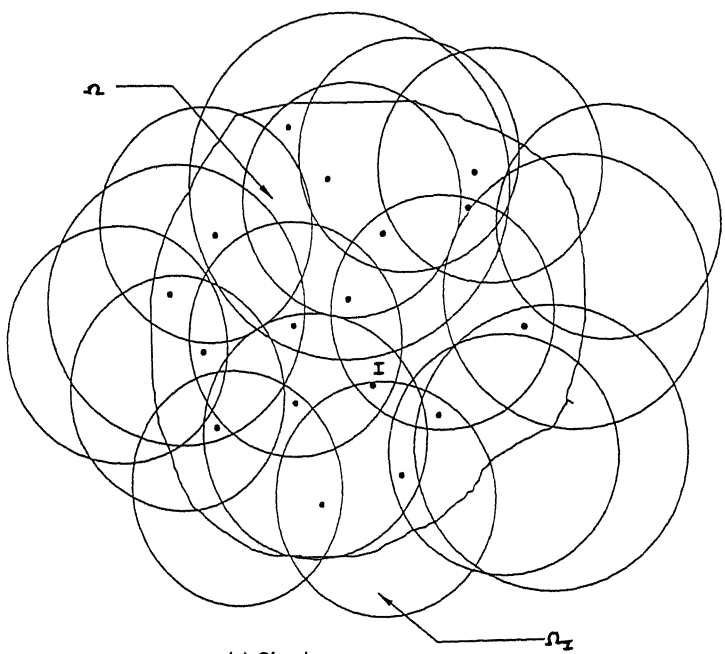

(a) Circular

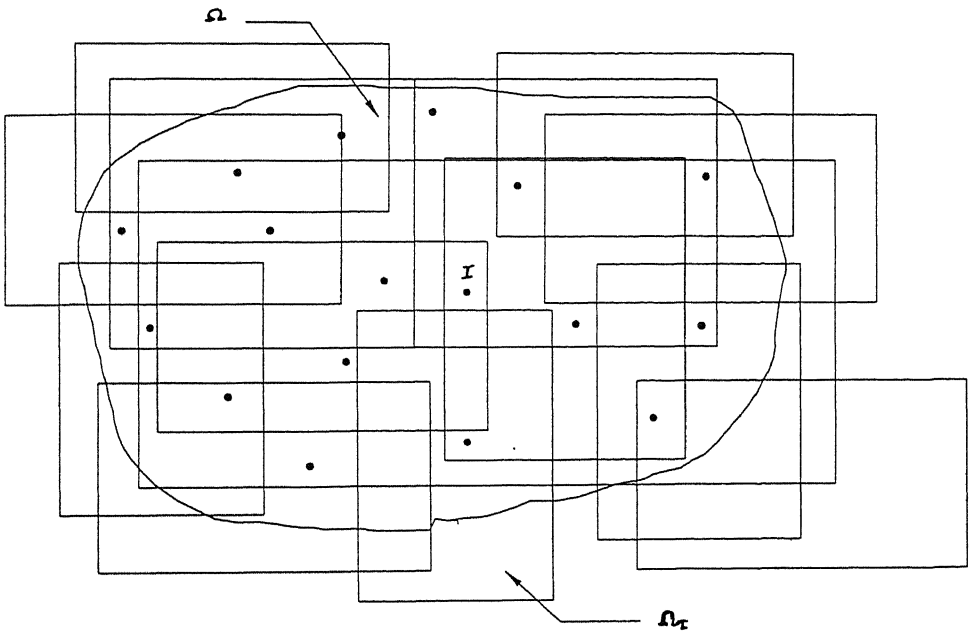

(b) Rectangular

Fig. 3.2 Domain of influence in two dimensions

An important ingredient of EFGM or the meshless methods is the weight function, $w(x)$. The choice of weight function can affect the MLS approximation of the $u^h(x)$. In this analysis, the Gaussian weight function has the form,

$$\text{Gaussian: } w(d_I) = \begin{cases} \dfrac{\exp\left(-\left(\dfrac{d_I}{c}\right)^2\right) - \exp\left(-\left(\dfrac{d_{mI}}{c}\right)^2\right)}{1 - \exp\left(-\left(\dfrac{d_{mI}}{c}\right)^2\right)} & d_I \le d_{mI} \\ 0 & d_I > d_{mI} \end{cases}$$

where $d_I = \|x - x_I\|$ is the distance from a sampling point x to a node x_I, and d_{mI} is the domain of influence of a node, i.e., the area for which the weight function is nonzero. The variable c in the Gaussian weight is used to control the dilation of the weight function. It is useful to define a characteristic nodal spacing, c_I, which is a

distance such that a node will yield a minimum set of neighbors sufficient for regularity of the equations used to determine the approximant. The weight function parameters are defined in terms of c_I

$$d_{mI} = d_{\max} c_I \qquad \ldots\ldots (3.27)$$

$$c = \alpha c_I \qquad \ldots\ldots (3.28)$$

where $d_{\max}$ and α are constants.

For the Gaussian weight function in the equation, the parameter α is a dilation parameter, which controls the shape of the weight function. If α is kept constant while $d_{\max}$ is increased, the shape of the weight function will not change and the effective domain of influence will be smaller than the actual domain of influence. It is necessary to have the ratio $\frac{d_{\max}}{\alpha} \geq 4.0$ to avoid poorly formed shape functions [Belystchko,1998]. In addition, α>0.5 is needed for smooth shape functions and derivatives.

3.6 Evaluation of Integrals

Computing the stiffness matrix and force vector from equation requires integration over the domain Ω, which, in two dimensions corresponds to area integration. Integrating the stiffness matrix and force vector requires a numerical integration scheme such as Gauss quadrature, which in turn, requires a subdivision of the domain. Since meshless methods have no inherent subdivision of the domain like finite elements, it is necessary to introduce subdivisions as shown in Fig.3.3. The first one shown, which matches the domain; this technique is often called an element quadrature .The vertices of this background mesh are often used as the initial array such as the nodes at the crack tip in the model shown.

The second integration technique, which is often called cell quadrature, uses a background grid of cells, which is independent of the domain. At each integration

point it is necessary to determine if it lies inside the domain before it is used for integrating equation. This technique is not widely used because it does not yield good accuracy along curved and angled boundaries.

To perform the quadrature, the domain of influence of each quadrature point must be determined. The domain of influence of a point never extends across any boundaries. Thus, for a quadrature point near a crack, the domain of influence of x_Q is limited to those points x_I that can be connected to x_Q without interesting a boundary of the domain. The contributions of a quadrature point to the linear equations depend on the nodes in the domain of influence of the point x_Q.

Domain of influence

Properly choosing the domain of influence or nodal support is an important aspect of meshless methods. The size of the support should be sufficiently large so that the moment matrix is regular and well conditioned and that the spatial distribution of neighbors is fairly even. On the other hand, choosing domains of influence that are too large leads to a great deal of computational expense in forming the approximations as well as assembling the stiffness matrix. Support sizes, which are too large, also detract from the local character of the approximation; for problems involving sharp gradients, some loss of accuracy is typically noted as the effect of the gradient is smeared.

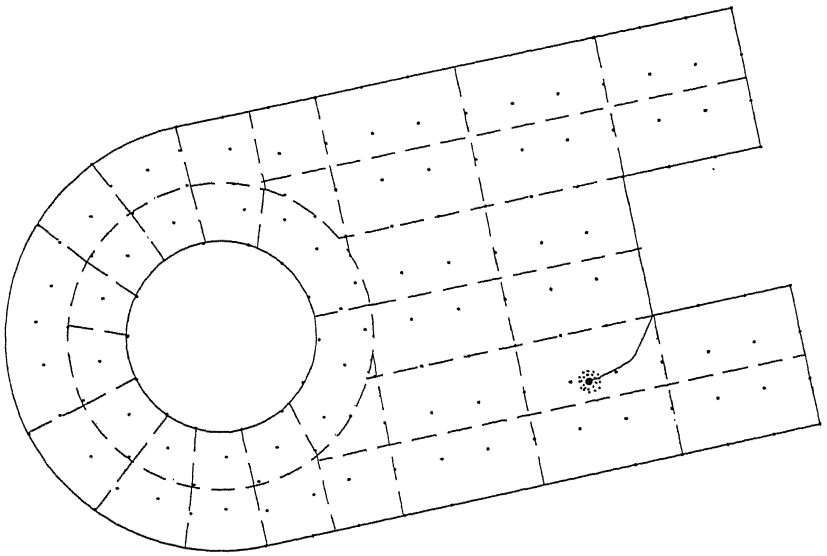

(a) Element quadrature

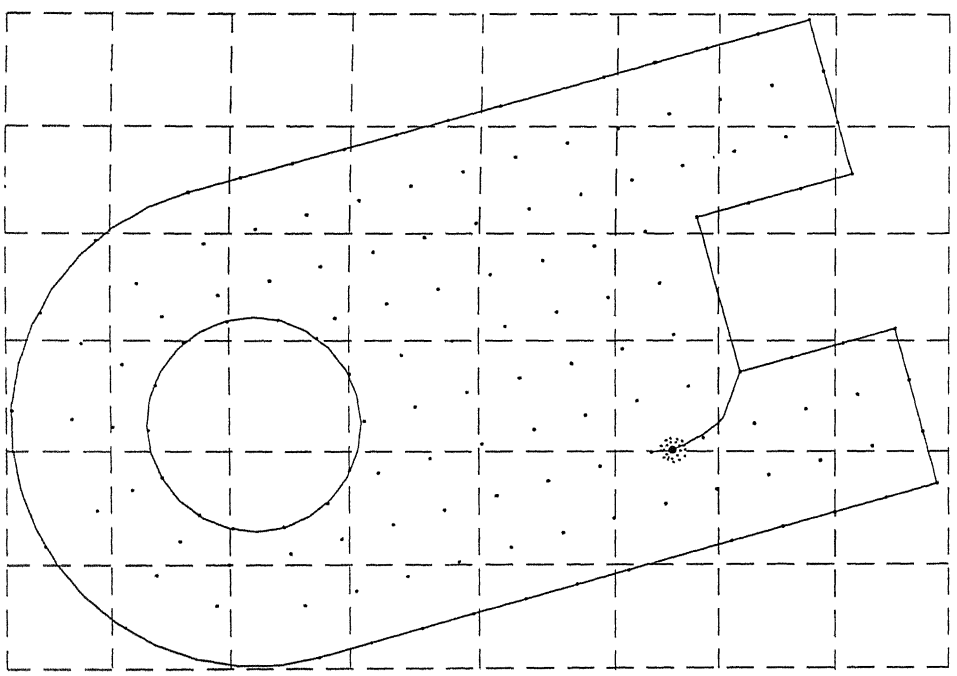

(b) Cell quadrature

Fig. 3.3 Two integration methods for integrating weak form of mesh less

3.7 Smoothing of EFG approximations

3.7.1 Introduction

The smoothness, which is inherent in meshless methods, has two important features. It provides approximation of functions and their derivatives, which are smooth and have the same continuity as the weight function. However, in cases where a discontinuity is present in either the geometry or the material, this higher order smoothness leads to difficulties that must be addressed in order to obtain good accuracy. Discontinuity occurs along an interface between two materials with different properties, leading to discontinuous strains across the interface. This situation is easily modeled using finite element where the interpellants are C_0. Cordes (1996) have solved problems with multiple material is using EFG by treating the individual material as separate bodies and joining them together with Lagrange multipliers. Belytschko (1997) have developed techniques in which a so-called jump term is included in the trial function that is capable of representing the discontinuity. The magnitude of the jump becomes an unknown in the Galerkin discretization.

The second class of problems, which contain discontinuities, are due to geometrical effects. This includes cases where a boundary of the geometry is nonconvex, such as a body with a hole or a crack. Because of the aforementioned smoothness of meshless methods, special procedures are required near nonconvex boundaries. There are technique to handle the nonconvex problem are visibility criterion, diffraction, transparency and see-through. We will use the diffraction method.

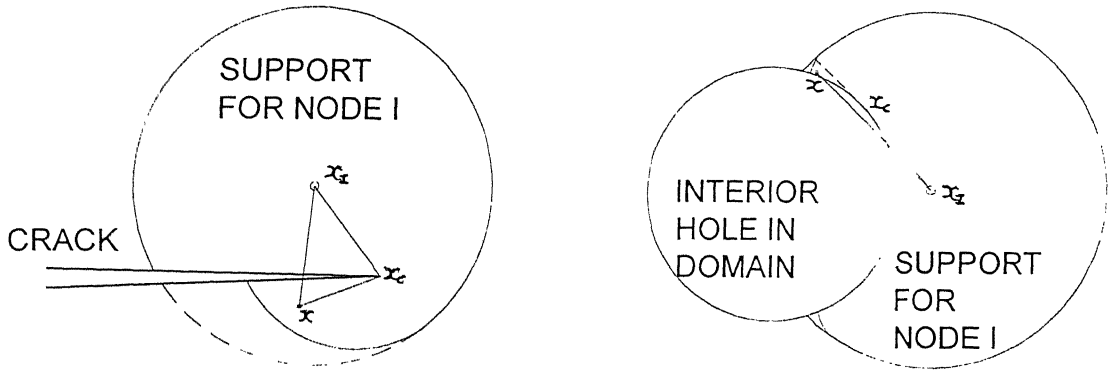

(a) Support around a crack tip

(b) Support around a hole

Fig. 3.4 Diffraction method for construction smooth weight function

3.7.2 Diffraction Method

Continuous and smooth approximants near nonconvex boundaries can be constructed quite easily by the diffraction method Organ (1996). The nodal support is wrapped around nonconvex boundaries similar to the way light diffracts around sharp corners. This method, which has also been called the wrap around method, is quite general and can be used for cracks or smooth boundaries such as interior holes. For example, in Fig.3.4, where a line between the node, X_I, and a sampling point, X, intersects a crack and the tip is within the domain of influence of the node. The weight function distance, d_I, is modified by

$$d_I = \left(\frac{s_1 + s_2(X)}{s_0(X)} \right)^{\lambda} s_0(X)$$

where $s_1 = \|X_I - X_C\|$, $s_2(X) = \|X - X_C\|$, $s_0(X) = \|X - X_I\|$, and X_I is the node, X

is the sampling point, and X_C is the crack tip. The parameter λ is used to adjust the distance of the support on the opposite side of the crack.

The spatial derivatives of the weight function are computed using the chain rule:

$$\frac{\partial w}{\partial x_i} = \frac{\partial w}{\partial d_I}\frac{\partial d_I}{\partial x_i}$$

Since $\partial w / \partial d_I$ is unchanged, all that is necessary are expressions for $\partial d_I / \partial x_i$:

$$\frac{\partial d_I}{\partial x_i} = \lambda\left(\frac{s_1 + s_2}{s_0}\right)^{\lambda-1}\frac{\partial s_2}{\partial x_i} + (1-\lambda)\left(\frac{s_1 + s_2}{s_0}\right)^{\lambda}\frac{\partial s_0}{\partial x_i}$$

where

$$\frac{\partial s_0}{\partial x_i} = \frac{x_i - x_{Ii}}{s_0} \quad \text{and} \quad \frac{\partial s_2}{\partial x_i} = \frac{x_i - x_{ci}}{s_2}$$

The diffraction method works well for general nonconvex boundaries as well. Consider the case shown in the line between a node and a sampling point intersects the boundary of a hole. The tangent point between the node and the nonconvex boundary is used as wrap-around point, X_C and earlier equation is used to compute the weight function distance, d_I. Note that for this implementation of diffraction method, the segment $d_2(X)$ intersects the boundary.

One drawback of the smooth approximations is that the computed crack opening profile is not parabolic at the tip. The shape functions wrap around the crack tip and the crack in effectively shortened if the smoothing effect is too large or the mesh is too coarse, so the maximum stress is then not at the crack tip, but is shifted a small distance that depends on the mesh refinement. This effect can be reduced by increasing λ in the diffraction method.

4.8 Closure

The moving least square methodology is reviewed and used to construct discrete EFG approximation. The elastic static boundary value problem is presented along with its associated weak form. Approximation of the solution with EFG is presented and topics of nodal domains of influence and integration of weak form are discussed. It should be noted that the definition of a meshless method is one in which no predefined element connectivity exists for determining the approximant. Some confusion invarbly arises when the meshless approximant is used in Galerkin method. Integration of weak form is performed by Gauss quardrature, which requires some sort of integration cells. Although this detracts from the meshless nature of the method the background cell structure by no means destroys it. Smoothing of EFG approximation near nonconvex boundaries is presented. Without smoothing, EFG approximation near nonconvex boundaries such as crack tips will contain discontinuities, which extend into the domain. These discontinuities arise due to a sampling point grazes the boundary. The diffraction method smoothes EFG approximation by wrapping the nodal support a short distance around the point at which the discontinuity would begin.

CHAPTER 4

RESULTS & DISCUSSION

The present EFG method was applied to perform fracture mechanics analysis of both stationary and propagating crack. Both single (mode I) and mixed mode (mode I & II) conditions were considered and five examples are presented here. The results are organized as follows:

1.Convergence study

- Near tip stress
- Centrally located crack
  - Small
  - Long

2. Crack growth analysis

- Two symmetrical cracks
- Two unsymmetrical cracks

4.1 Convergence Study

A rectangular plate with an edge crack under pure tension is considered (Fig. 4.1). The far field applied traction is t_x † 1 unit. The mode I stress intensity factor K_{I} was evaluated by using the J integral. Due to symmetry, only half of the plate was analyzed. The plate is divided into 10×10 rectangular cells with their nodes coinciding with the meshless nodes (discussed in section 3.6) to facilitate the numerical integration. For all the cells, a 4×4 Gauss Quadrature was used except for the two around the crack tip, where 9×9 Gauss Quadrature was used to handle

the crack tip singularity. A plane stress condition was assumed with $E = 207000$ and $\upsilon = 0.3$.

The value of stress intensity factor for mode I as a function of the crack length is given in the Table 4.1. As can be seen, the computed stress intensity factor agrees with the exact values of K_I for all values of crack length. The percentage error in stress intensity factor K_I is found to be equal to 1.229%.

Apart from the crack length, the accuracy of stress intensity factor also depends upon the additional number of nodes around the crack tip. The effect of additional number of nodes and basis on stress intensity factor is compare in the Table 4.2. It is observed, that as the additional number of nodes increases the error goes down (Table 4.2) and this also shows the effect of linear and quadratic basis assumption. In linear basis assumption, zero additional node percentage error is equal to 16.01% and as go on 15 additional nodes this is reduced to 1.23%. In quadratic basis assumption, zero additional node percentage error is equal to 13.02% and as go on 15 additional nodes this is reduced to 1.15%.

Near tip stress for mode I

The near tip stress field of a crack of size, 2a=1 unit. Containing an edge crack of a=0.5 unit is investigated. The meshless discretization (nodes) is shown in Fig. 4.1(a.). The objective is to predict the near tip stress field by meshless method and to compare with corresponding LFEM field. A plane stress condition was assumed with the same value of E and υ. For evaluation of stress, linear basis with 15 additional nodes is used.

Fig. 4.2 shows the plot of radial (σ_{rr}) and circumferential $(\sigma_{r\theta})$ stress as a function of r/a for the range of 0.005 to 0.20, with θ † 0°. The error between predicted stress values from the meshless method and the exact values is within 2%. Fig. 4.2 shows the plot of radial (σ_{rr}), circumferential $(\sigma_{r\theta})$ and shear $(\tau_{r\theta})$ stress as a function of θ when $r/a = 0.08$. The error between predicted stress values from the meshless method and the exact values is within 2%.

Centrally located straight edge crack

- **Small crack**

A centrally located small cracked plate with the following initial parameters and location of crack is given in Fig. 4.4

Domain = $5 \times 3.5\ cm^2$

Crack length = $0.5\ cm$

- **Long crack**

A centrally located long cracked plate with the following initial parameters location of crack is given in Fig. 4.5.

Domain = $5 \times 3.5\ cm^2$

Crack length = $1.0\ cm$

To verify the robustness of method, results were compared for different values of crack length.

For both the problems, the theoretical values of K_{I} and K_{II} for the finite plate after applying the finite plate correction factor agree within the range of 0.5% with the values obtained from meshless method Table 4.3.

4.2 Crack Growth Analysis

One of the biggest benefits of the meshless methods such, as EFG is their inherent ability to model arbitrary crack propagation due to the absence of predefined element connectivity. Growing a crack consists of simply adding another line segment at the existing crack tip as shown in Fig. 4.3. The direction and the growth rate are determined by the principles of the fracture mechanics, which was discussed in earlier chapter.

First of all, a node has to be located at the crack tip. This node is actually placed a short distance ahead of the tip of the crack. As the crack propagates, it will pass directly through the current crack tip node and may pass through other nodes as well. In this case, two nodes replace the node, one above the crack and another below the crack. This is preferred to deleting the node because it increases the spatial resolution along the crack surface. The meshes were constructed by simply translating the dense pattern around the crack tip through the fixed mesh representing the geometry, dividing any node passed by the crack into two and displacing them normal to the crack surface by a distance $10^{-4}w$.

Two symmetrical located

The symmetrically located straight cracks with the following initial parameters and the location of crack given in the Fig. 4.6.

Domain $=5\times 3.5\ cm^2$

After each iteration, the crack profile is given the proper crack extension in the right direction and the whole analysis is repeated. The stress intensity factor is given in Table 4.4. The corresponding crack geometries at the beginning of the each step are shown in the Figure (4.6-4.9).

1. Following the theoretical analysis for same geometry and location of crack, both the crack should be propagating in a straight line. This is also what was observed the present analysis.

2. As crack grows, the interaction between two cracks becomes more severe leading to an increase in stress intensity factor.

Two unsymmetrical located

The unsymmetrical located straight cracks with the following initial parameters and location of crack in given in figure 4.10.

Domain $=5\times3.5\ cm^2$

After each iteration, the crack profile is given the proper crack extension in the right direction and the whole analysis is repeated. The stress intensity factor is given in the Table (4.5-4.6). The corresponding crack geometries at the beginning of the each step are shown in Figure (4.11-4.19).

After each iteration, the analysis is repeated by another basis, which is quadratic, and compare the results in the Figure (4.20-4.23) and Table (4.5-4.6).

1. As the cracks grow, the interaction between the two cracks increases leading to an increase in the observed stress intensity factor values.

2. The cracks tend to turn towards each other. So the intuitive reasoning that near the boundary, the crack will tend to grow towards the region of high stress concentration.

3. The mixed mode stress intensity factor is mainly K_I dominated. Mode II is important for the point of view of orientation of the crack growth direction. The crack turns primarily due to K_{II} .

4. Difference between the different basis is evaluation is very less and so quadratic or higher degree basis can be sweep by raising the number of node around the crack tip.

Table 4.1: Stress intensity factor for the edge crack problem

Crack length (a)	K_I	K_{exact}	% Error
0.20	1.078	1.086	0.736
0.24	1.249	1.278	2.269
0.28	1.481	1.493	0.803
0.32	1.722	1.737	0.863
0.36	2.073	2.021	2.572
0.40	2.329	2.358	1.229

Table 4.2: Stress intensity factor comparison for edge crack

Additional Node	**Basis**			
	Linear		**Quadratic**	
	K_I	K_I / K_{exact}	K_I	K_I / K_{exact}
0	1.9807	0.8399	2.051	0.8698
5	2.2122	0.9381	2.284	0.9686
15	2.329	0.9877	2.3308	0.9885

Table 4.3: Comparison of the exact and calculated value of S.I.F.

Type of crack	K_I	K_{exact}	K_{II}	K_{exact}
Small	0.8955	0.8963	-0.00072	0.0000
Long	1.2757	1.2862	-0.00264	0.0000

Table 4.4: Comparison the S.I.F. for symmetrical crack problem

Step	Linear			Quadratic		
	K_I	K_{II}	θ	K_I	K_{II}	θ
1	0.8487	-0.00023	0.031	0.8503	-0.00024	0.032
	0.8653	-0.00024	0.032	0.8679	-0.00026	0.034
2	0.8429	-0.00017	0.026	0.8511	-0.00019	0.026
	0.8726	-0.00048	0.062	0.8806	-0.00041	0.054
3	0.9216	-0.00053	0.068	0.9249	-0.00067	0.083
	1.005	-0.00139	0.158	1.0092	-0.00147	0.167

Table 4.5: Comparison the S.I.F. for unsymmetrical crack problem

Step	Linear		Quadratic		% Difference	
	K_I	K_{II}	K_I	K_{II}	K_I	K_{II}
1	0.8343	0.0121	0.8349	0.0122	-0.07192	-0.82645
	0.8527	0.0113	0.8561	0.0119	-0.39873	-5.30973
2	0.8318	0.00561	0.8321	0.00567	-0.03607	-1.06952
	0.8588	0.00731	0.8602	0.00789	-0.16302	-7.93434
3	1.0021	-0.00162	1.019	-0.00145	-1.68646	10.49383
	1.0879	0.0072	1.0901	0.0064	-0.20222	11.11111
4	1.3614	-0.0219	1.3671	-0.0211	-0.41869	3.652968
	1.4608	-0.0318	1.4691	-0.0284	-0.56818	10.69182
5	1.7288	-0.0397	1.7341	-0.0403	-0.30657	-1.51134
	1.8547	-0.198	1.8613	-0.2028	-0.35585	-2.42424
6	2.0304	-0.0527	2.0706	-0.0556	-1.97991	-5.50285
	2.1568	-0.3365	2.1812	-0.3398	-1.13131	-0.98068
7	2.4817	-0.2238	2.4893	-0.2312	-0.30624	-3.30652
	2.5665	-.3191	2.5688	-0.3092	-0.08962	3.102476
8	2.9423	-0.3133	2.9512	-0.3183	-0.30248	-1.59591
	2.7168	-0.3087	2.7218	-0.3155	-0.18404	-2.20279
9	3.2987	-0.4210	3.3012	-0.4297	-0.07579	-2.06651
	2.992	-0.3942	3.002	-0.4011	-0.33422	-1.75038
10	3.6791	-0.4987	3.6912	-0.5135	-0.32888	-2.96772
	3.2147	-0.3782	3.3128	-0.3841	-3.05161	-1.56002

Table 4.6: Comparison the direction for unsymmetrical crack problem

Step	Linear	Quadratic	% Difference
	θ	θ	θ
1	-1.66	-1.674	-0.84337
	-1.52	-1.592	-4.73684
2	-0.777	-0.781	-0.5148
	-0.975	-1.051	-7.79487
3	0.185	0.163	11.89189
	-0.756	-0.672	11.11111
4	1.845	1.768	4.173442
	2.49	2.213	11.1245
5	2.52	2.66	-5.55556
	11.92	12.156	-1.97987
6	2.99	3.0702	-2.68227
	16.96	16.936	0.141509
7	10.15	10.437	-2.82759
	13.77	13.355	3.013798
8	11.89	12.04	-1.26156
	12.64	12.89	-1.97785
9	14.10	14.366	-1.88652
	14.52	14.719	-1.37052
10	14.92	15.275	-2.37936
	13.07	12.893	1.354246

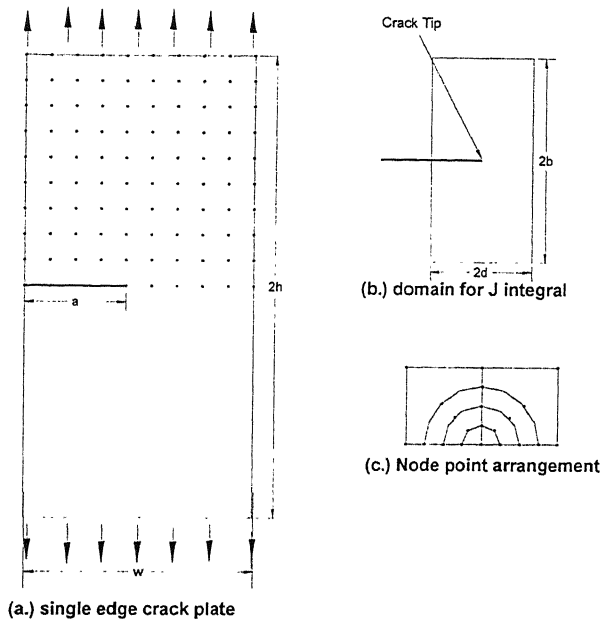

Fig.4.1 Single edge cracked plate

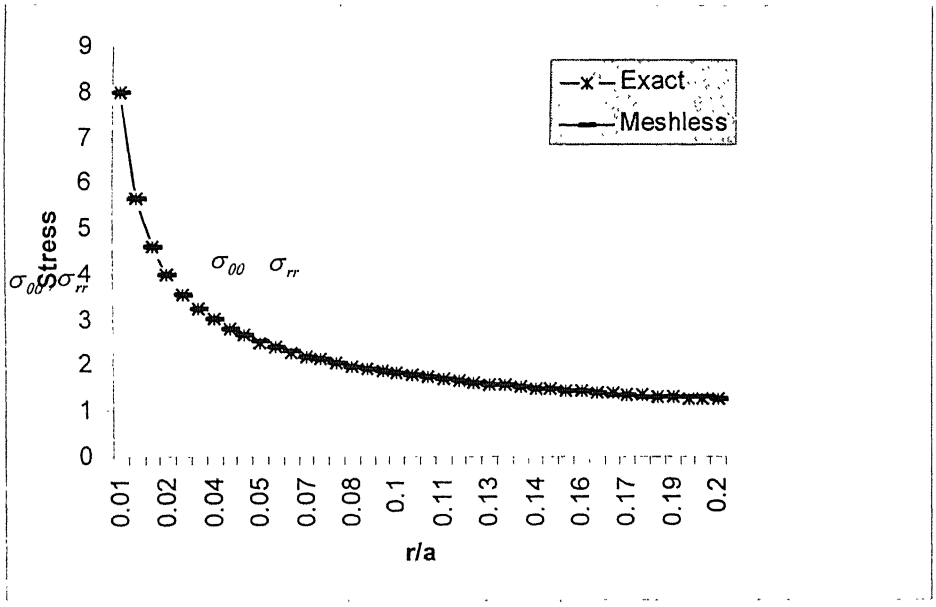

Fig. 4.2(a.) Near crack tip stress field for θ=0

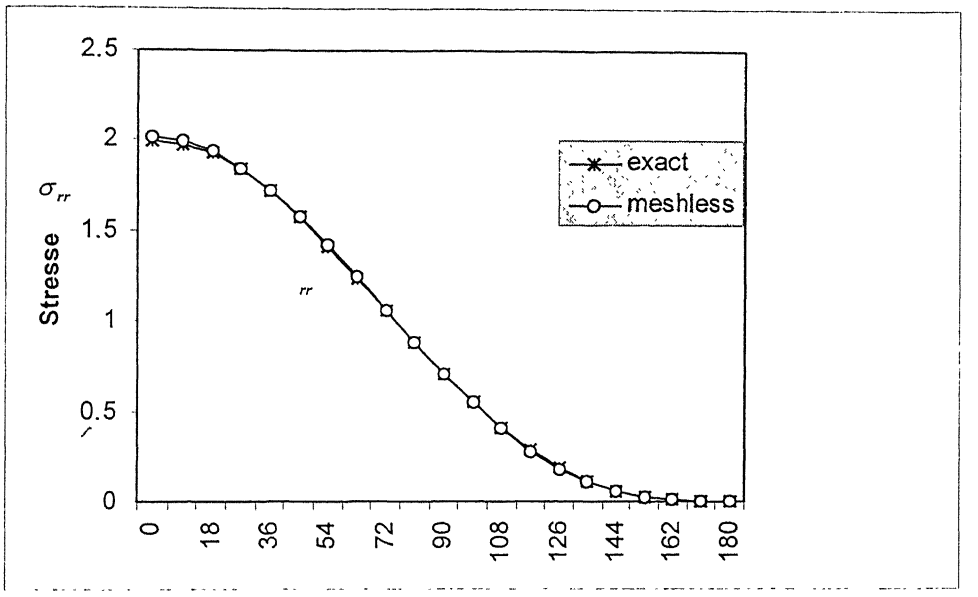

Fig.4.2(b.) angular variation of stress for r/a = 0.08

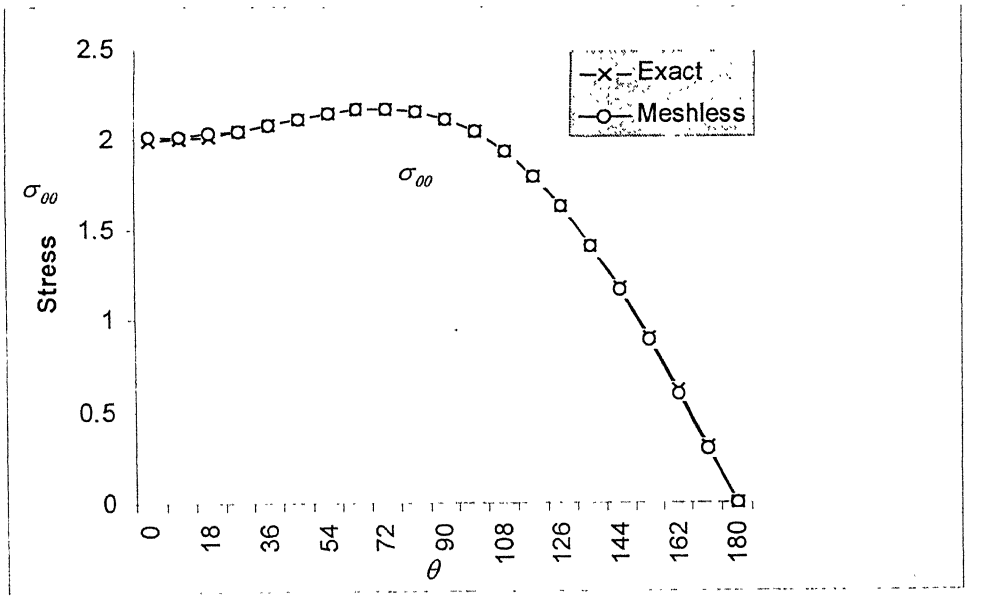

Fig. 4.2(c.) angular variation of stress for r/a = 0.08

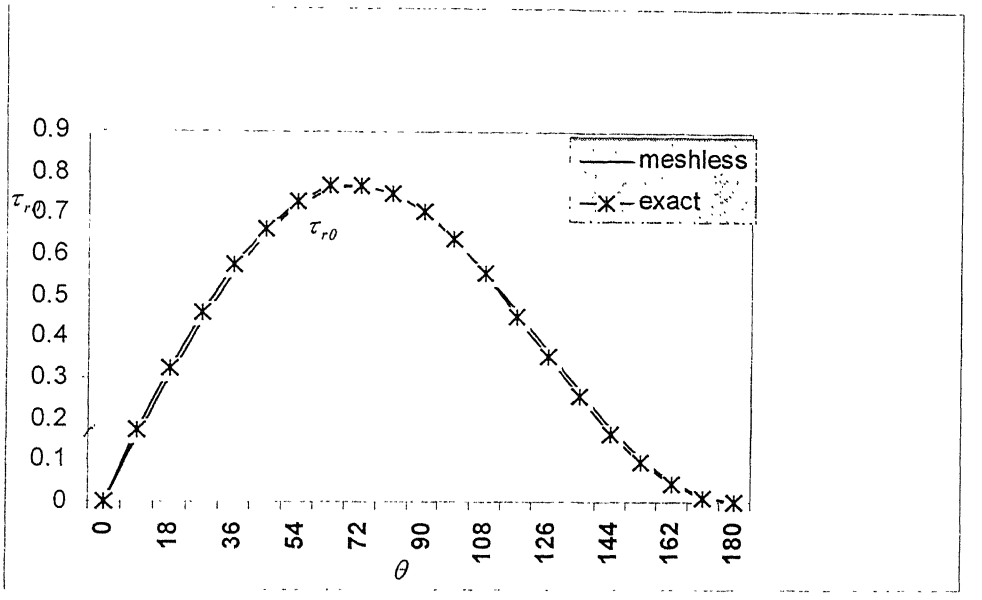

Fig. 4.2(d.) angular variation of stress for r/a = 0.08

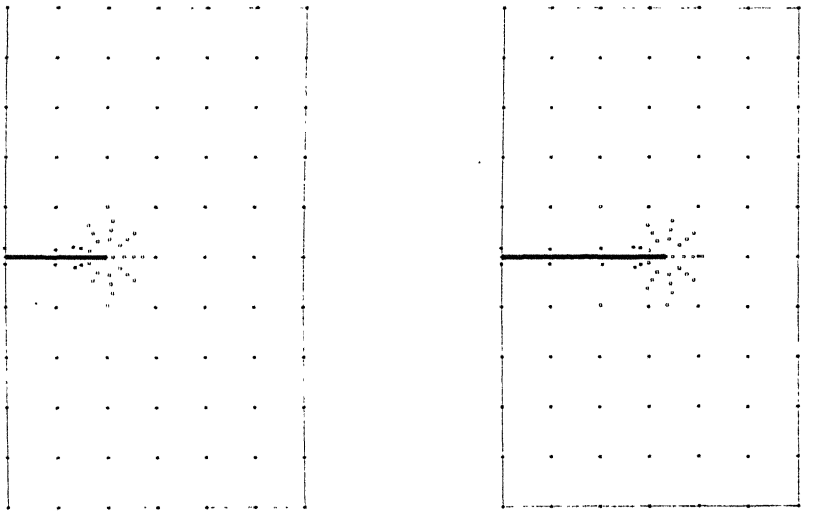

mesh arrangement

Fig. 4.3 Meshes for the progressive growth of edge crack problem

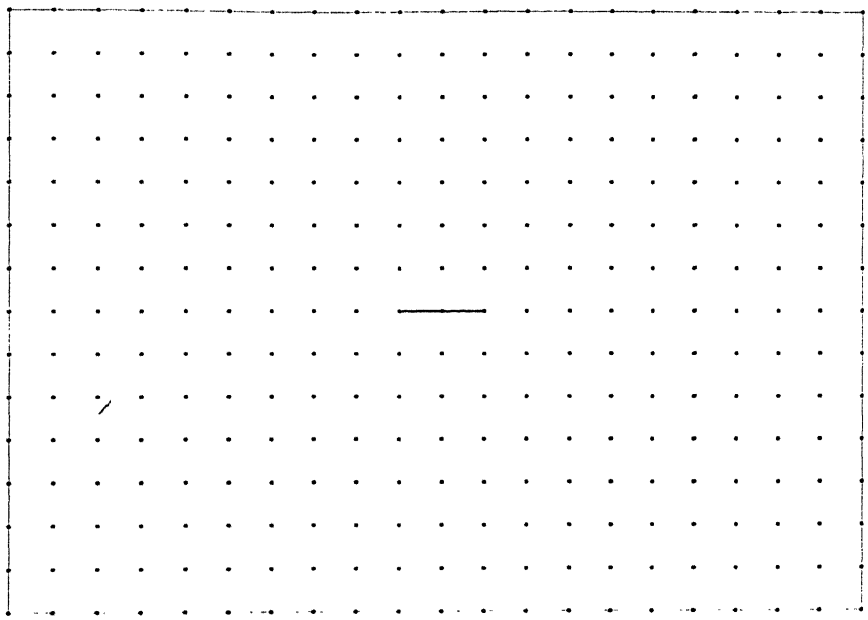

Fig. 4.4 Straight edge small crack

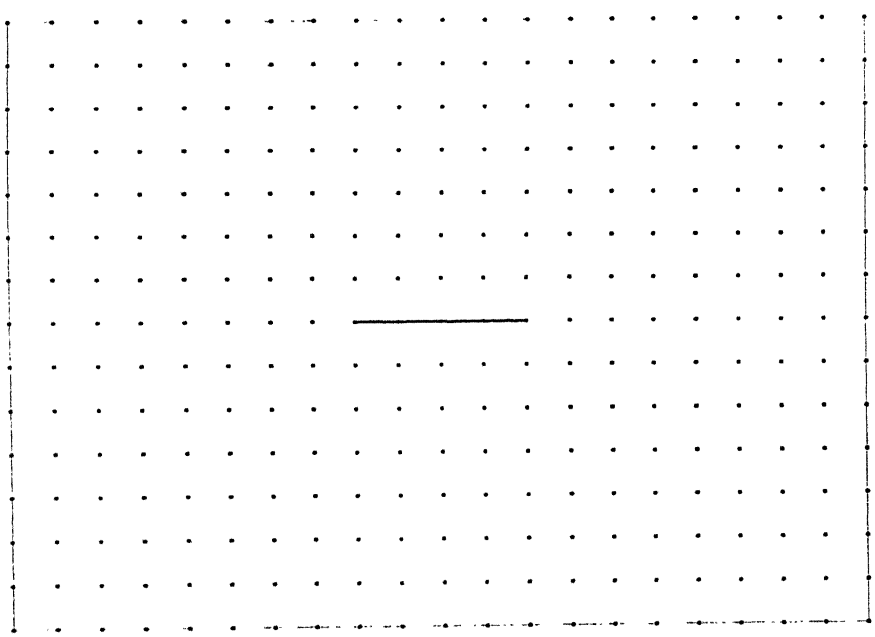

Fig. 4.5 Straight edge long crack

Step 1

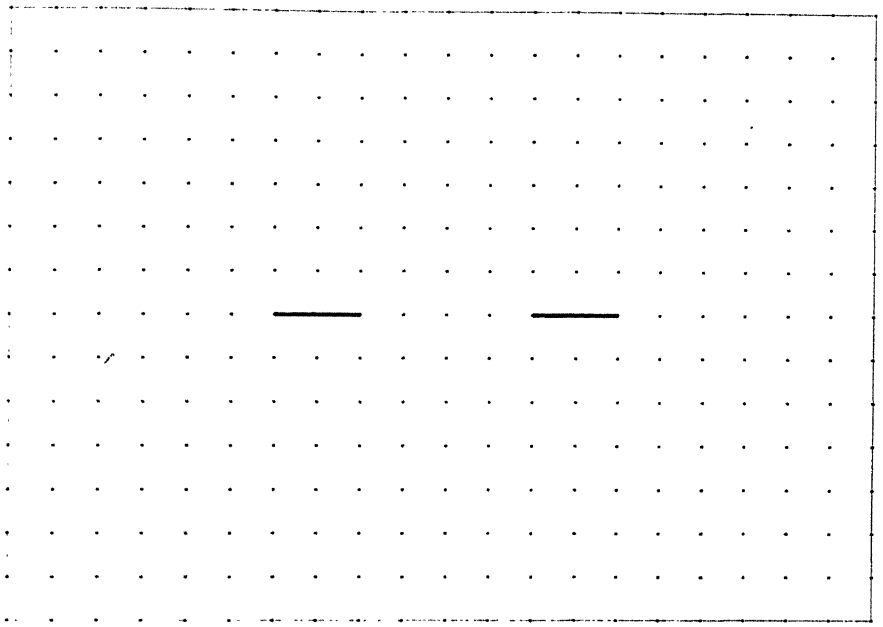

Fig 4.6 Problem 1 growth step 1

Step 2

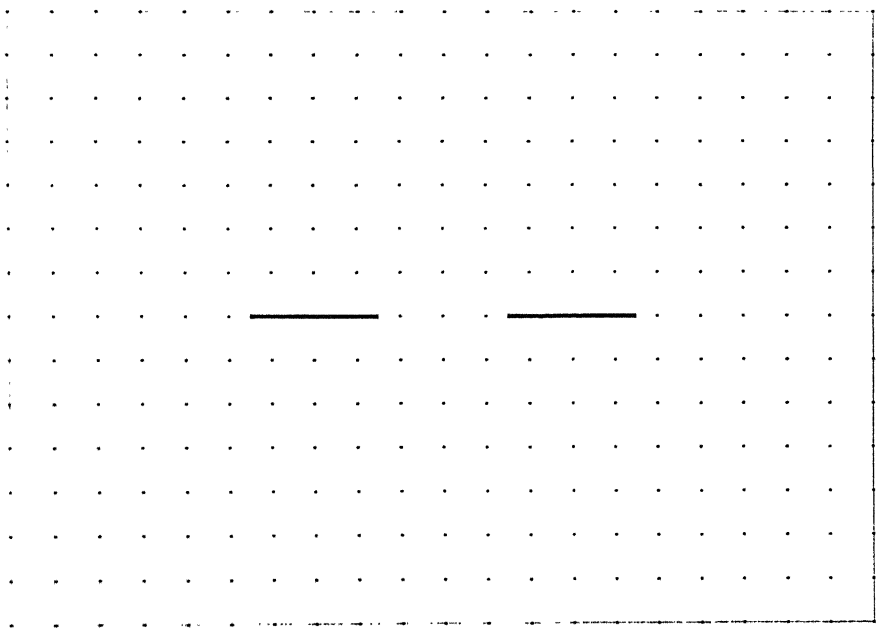

Fig 4.7 Problem 1 growth step 2

Step 3

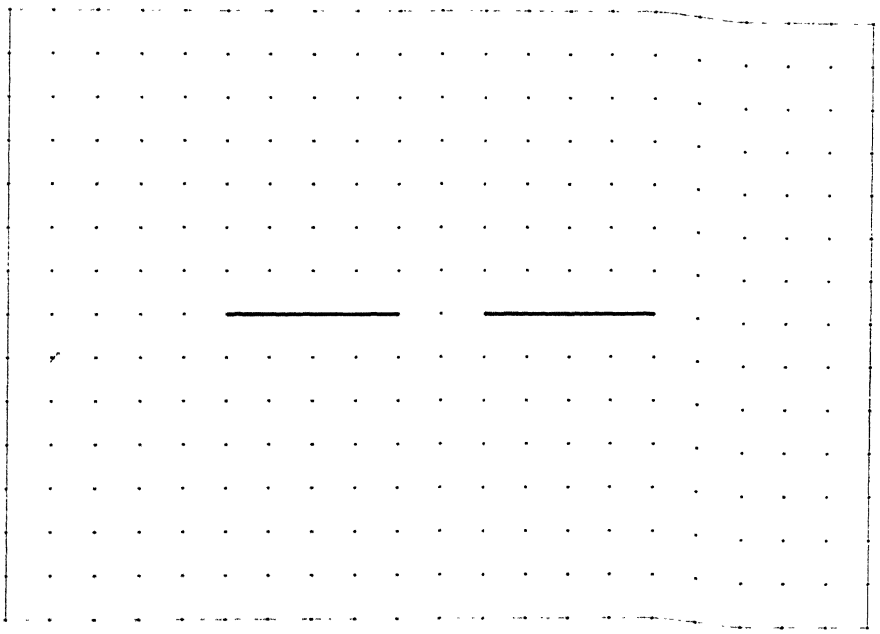

Fig 4.8 Problem 1 growth step 3

Step 4

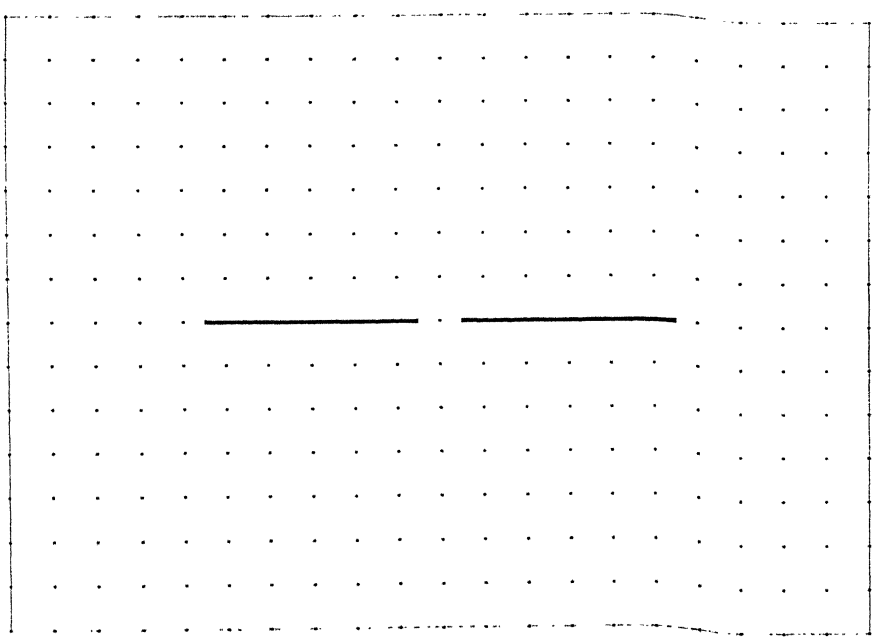

Fig 4.9 Problem 1 growth step 4

Step1

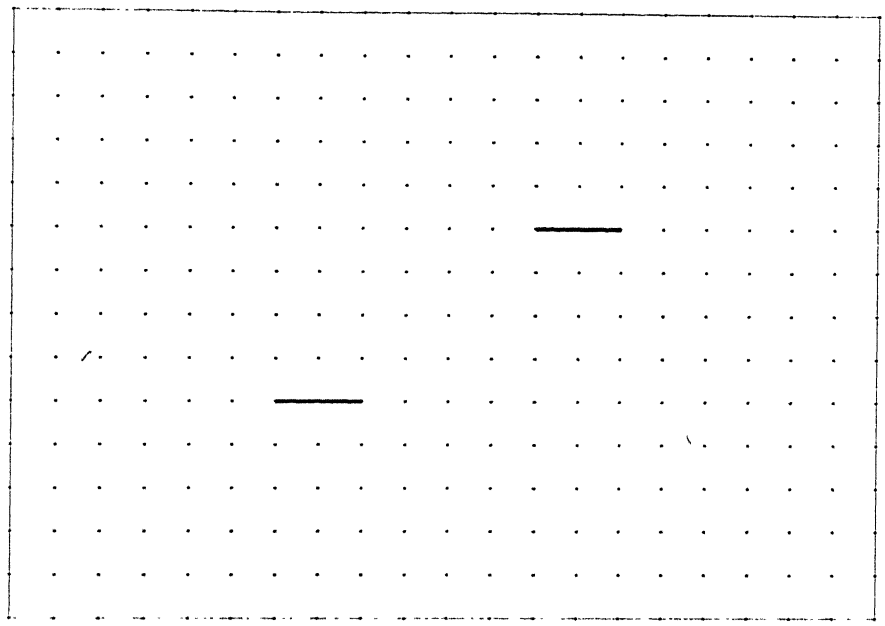

Fig 4.10 Problem 2 growth step 1

Step2

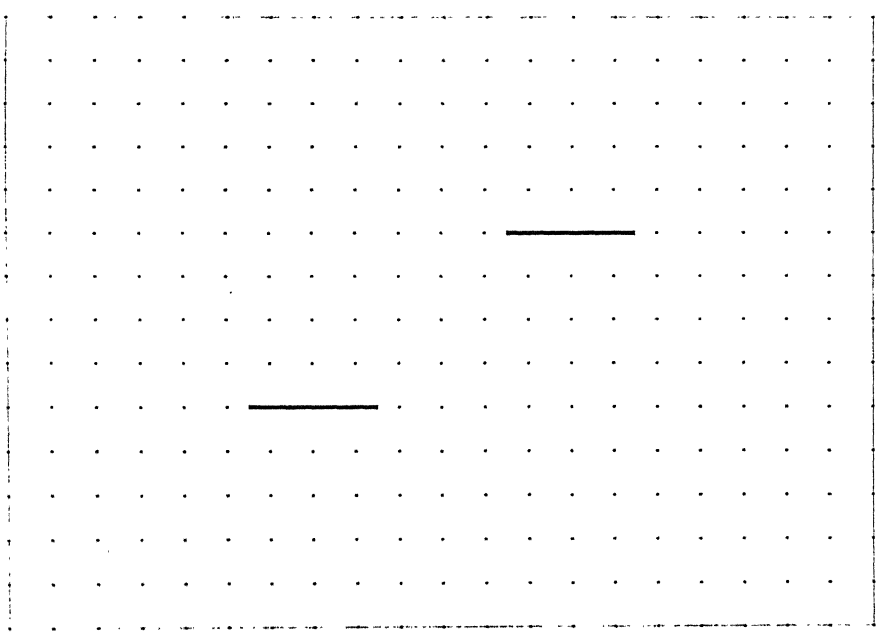

Fig 4.11 Problem 2 growth step 2

Step 3

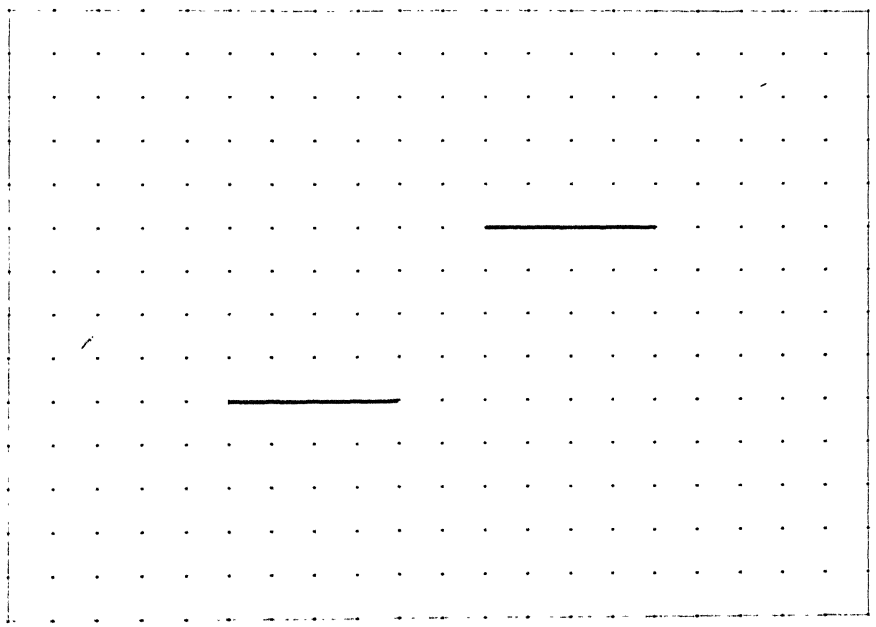

Fig 4.12 Problem 2 growth step 3

Step 4

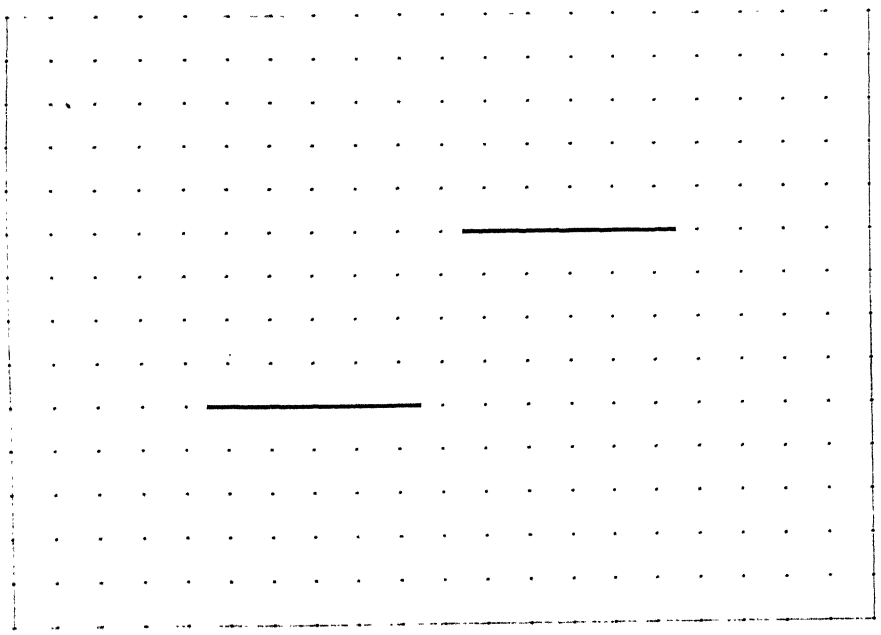

Fig 4.13 Problem 2 growth step 4

Step 5

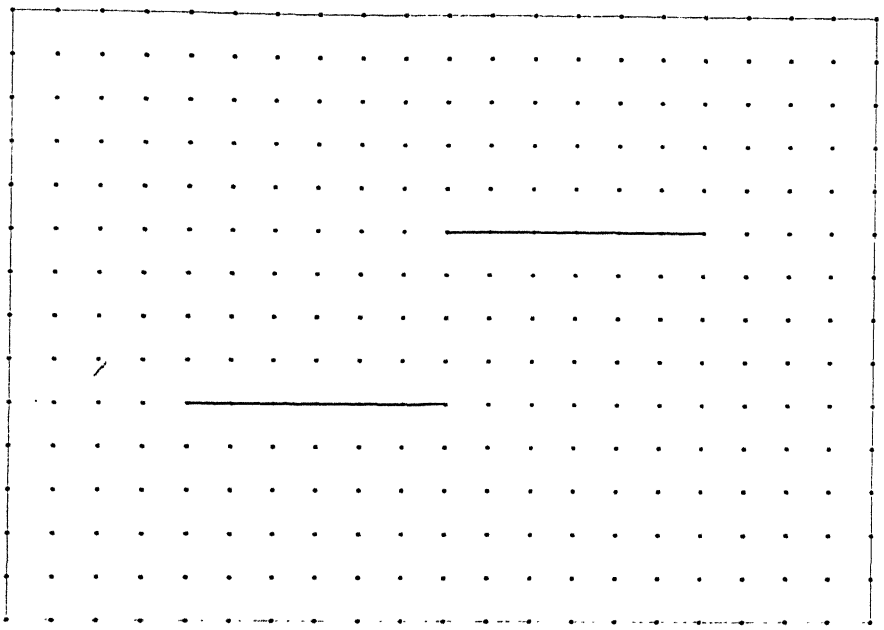

Fig 4.14 Problem 2 growth step 5

Step 6

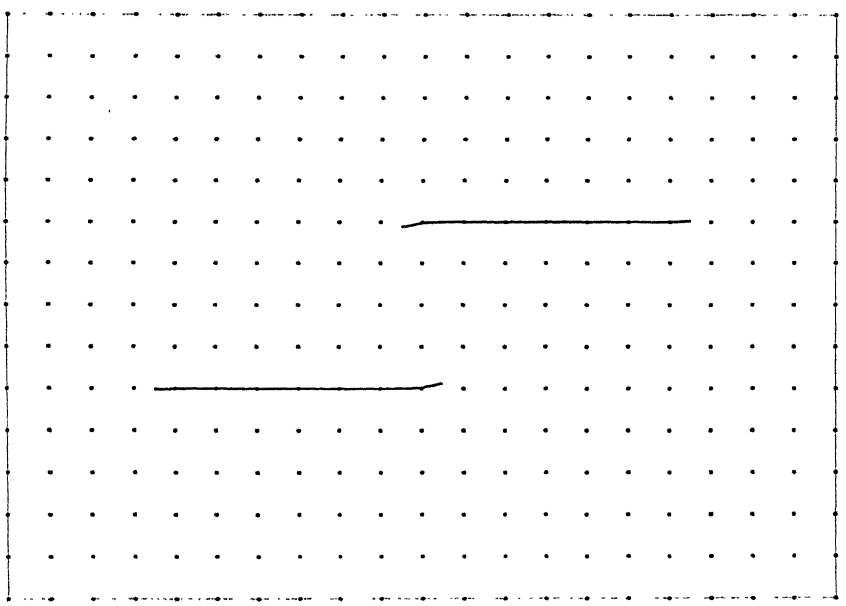

Fig 4.15 Problem 2 growth step 6

Step 7

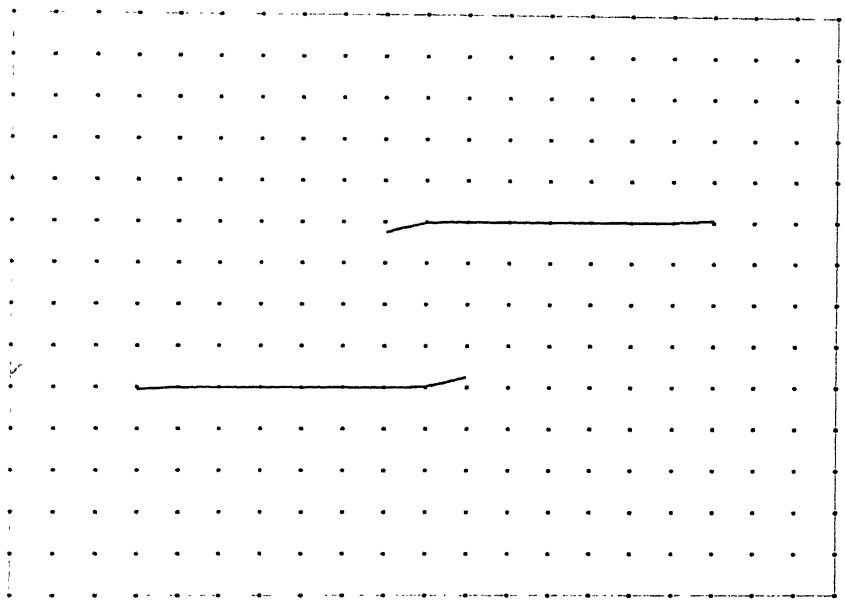

Fig 4.16 Problem 2 growth step 7

Step 8

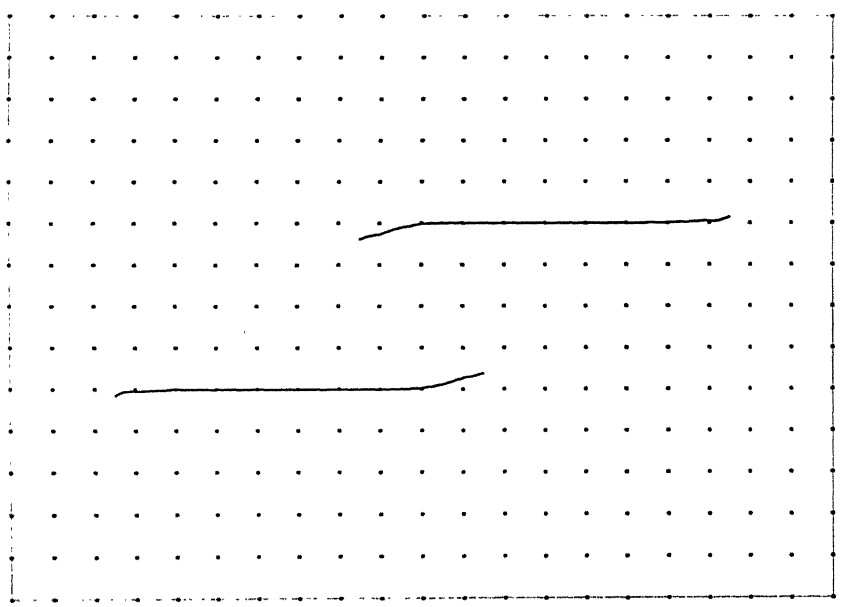

Fig 4.17 Problem 2 growth step 8

Step 9

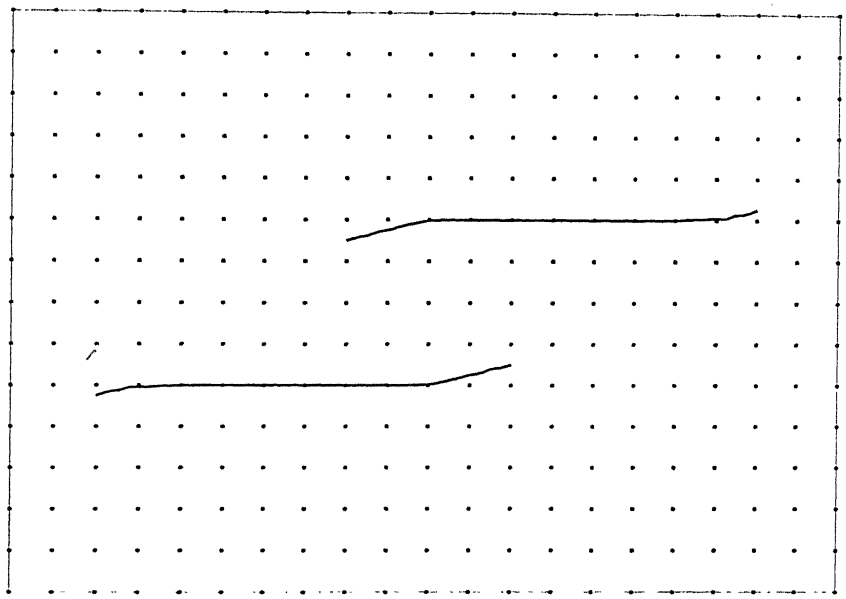

Fig 4.18 Problem 2 growth step 9

Step 10

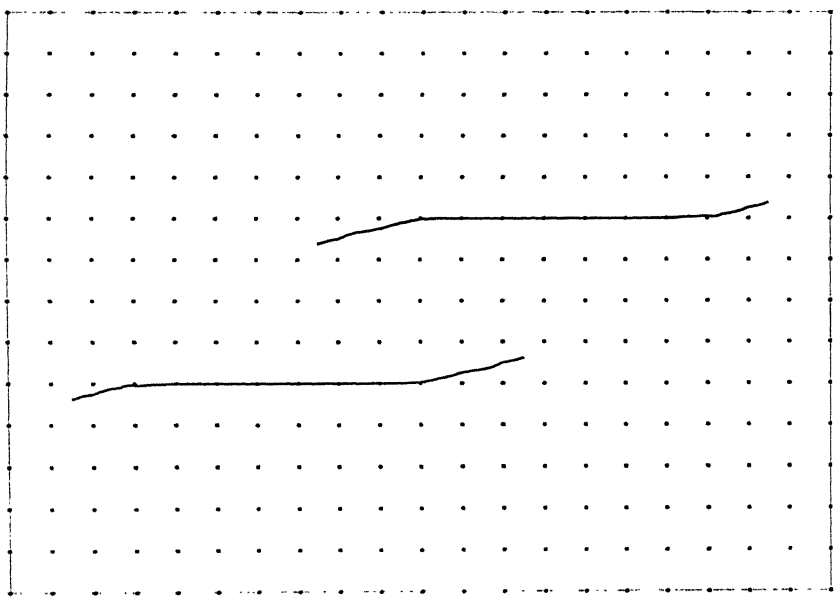

Fig 4.19 Problem 2 growth step 10

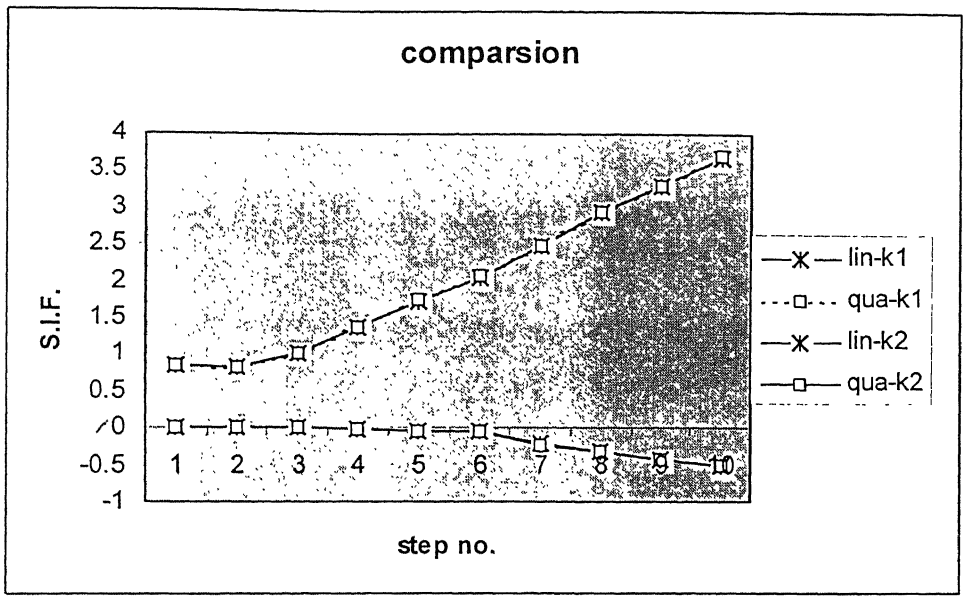

Fig. 4.20 Problem 2 comparison of S.I.F. at different basis

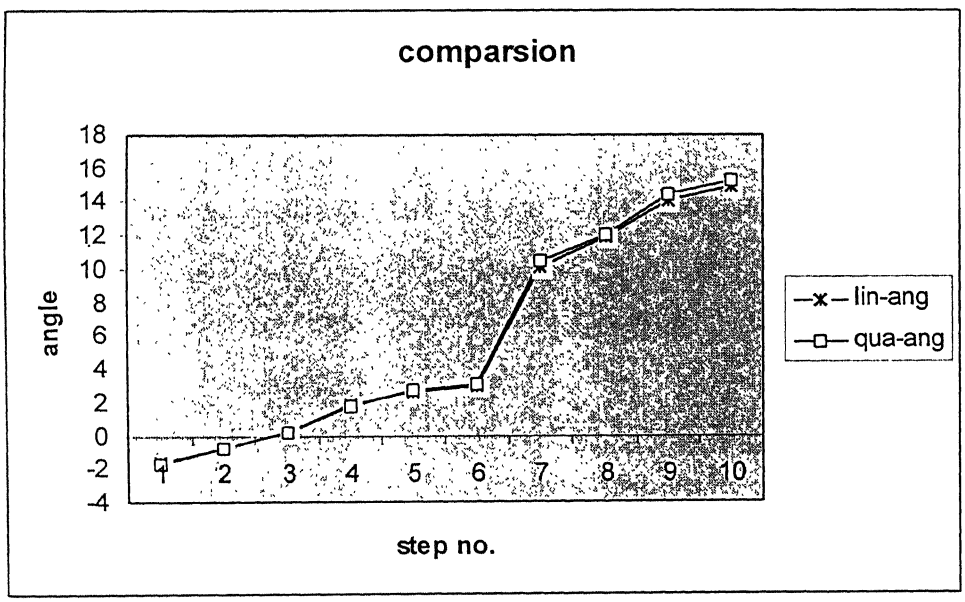

Fig. 4.21 Problem 2 comparison of angle at different basis

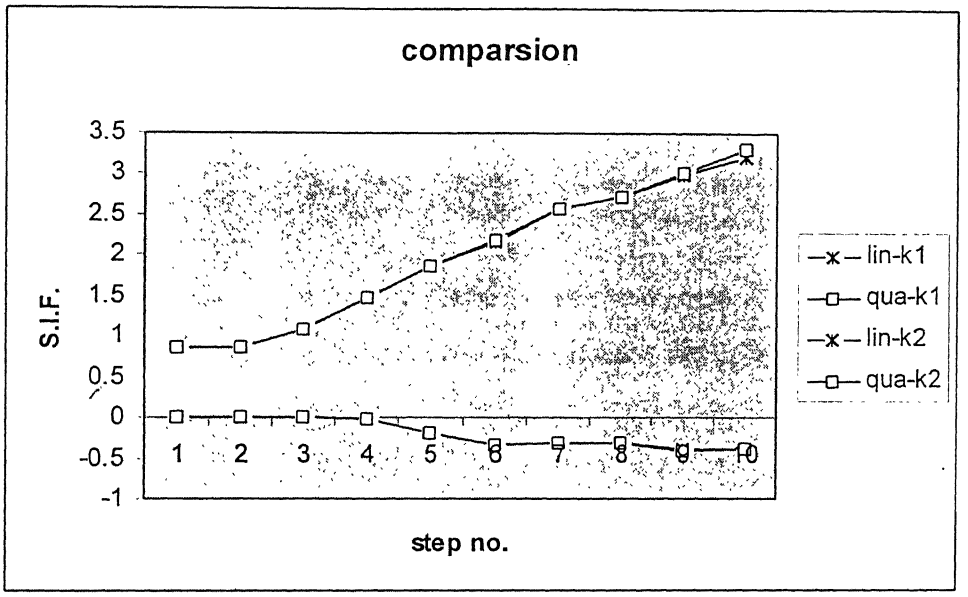

Fig. 4.22 Problem 2 comparison of S.I.F. at different basis

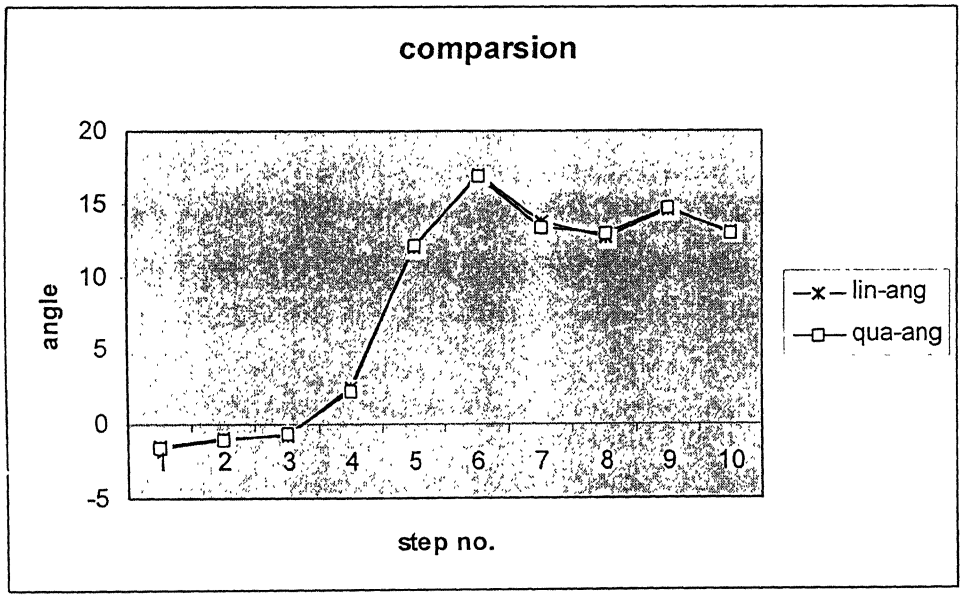

Fig. 4.23 Problem 2 comparison of angle at different basis

CHAPTER 5

CONCLUSIONS

5.1 Conclusions

An Element Free Galerkin method (EFG) has been developed to analyze 2-D fracture problems. This method can determine crack singularity in mode I & II and predict crack propagation. Several studies have been presented of different crack geometries and EFG method parameter.

Based on the studies the following conclusions are drawn:

1.The application EFG to fracture is very accurate and computationally very efficient. The SIF (K_I) is accurate and has error below 2% for linear basis and 1% for quadratic basis assumption.

2. The crack propagation direction is accurate and has error less than 2%. This became possible with moderate mesh configuration.

3.Unlike BEM or FEM, the EFG method does not need the crack to propagate only along the element edges. That way, any arbitrary propagation direction of the crack can be predicted.

5.2 Suggestions For The Future Work

1. Further studies, regarding the other basis functions and weighting functions can be explored for more efficient algorithms.

2. The method can be extended to analyze dynamic fracture problems and elasto-plastic material fracture problems.

References

1. *Lancaster, P. and K. Salkauskas* (1981). Surfaces Generated by Moving Least Squares Methods. *Mathematics of Computation* 37, 141-158.

2. *Belytschko, T., Y. Krongauz, D. Organ, M.Fleming, and P. Krysl* (1996). Meshless methods: An overview and recent developments. *Computer Methods in Applied Mechanics and Engineering* 139, 3-47.

3. *Belytschko, T., Y. Y. Lu, and L. Gu* (1994). Element-free Galerkin methods. *International Journal for Numerical Methods in Engineering* 37, 229-256.

4. *Fleming, M., Y. Chu, B. Moran, and T. Belytschko* (1997). Enriched element-free Galerkin methods for crack tip fields. *International Journal for Numerical Methods in Engineering* 40, 1483-1504.

5. *Duarte, C. A. and J. T. Oden* (1996a). H-p clouds – an hp clouds meshless method. *Numerical Methods for Partial Differential Equations*, 1-34

6. *P. Kumar*, Elements of Fracture Mechanics, Wheeler Publication

7. *Lucy, L.* (1997) A numerical approach to testing the fission hypothesis. *Astron. J.* 82: 1013-1024

8.*Monaghan, J. J.* (1988) An introduction to SPH. *Comp. Phys. Commun.* 48: 89-96

9.*Schlangen, E. and J. G. M. Mier* (1992). Experimental and numerical analysis of strain concentration by notches and cracks. *Journal of Applied mechanics* 35, 379-386.

10. *Swenson, D. V. and A. R. Ingraffea* (1988). Modeling mixed mode dynamic crack propagation using finite elements: *Theory and applications. Computational Mechanics* 3, 381-397.